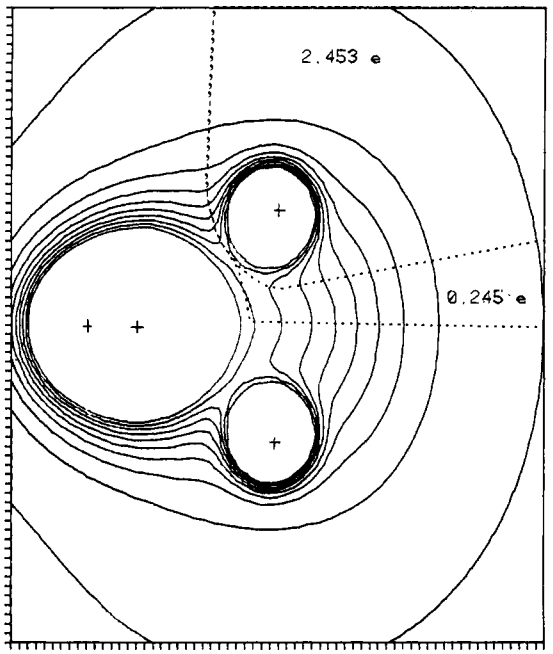

Figure 13. Projected electron density of the summation of Li_2 and triplet methylene with contour levels from 0.001 to 0.091 by 0.01 e au^{-2}. Dashed line is the demarcation line for tetrahedral triplet CH_2Li_2.

dilithiomethane with one electron in a Li–Li bonding orbital is being compared with a model having a two-electron Li–Li bond. Nevertheless, the model greatly assists in explaining the reversed dipole moment of the triplets. Triplet methylene has a dipole moment of 0.66 D with the hydrogen end being positive. Thus, the decrease of the positivity of the lithiums in the triplet state allows for the inherent dipole of triplet methylene to become significant, enough so as to actually reverse the direction of the dipole moment of dilithiomethane.

For a similar system, 1,1-dilithioethylene, a dipole moment reversal has been noted for the planar triplet and tetrahedral triplet states.[16] Their argument for explaining increased electron density about lithium in the triplets is similar to ours. However, it is not clear that a Mulliken population difference of 0.13 e between the singlet and the triplet is both an accurate expression of the electron population about lithium or sufficient for reversing the dipole moment. Triplet 1,1-dilithioethylene may be modeled as triplet vinylidene associated with Li_2 (analogous to our model for dilithiomethane). The inherent dipole moment of vinylidene is 0.43 D with the hydrogen end positive. Therefore, the dipole moment may reverse in the same fashion as for dilithiomethane; i.e., a decreased positivity of lithium allows the dipole moment contribution of triplet vinylidene to become dominant.

Acknowledgment. Preliminary calculations were done by G. W. Shriver. This research was supported in part by N.I.H. Grant No. GM-30369. The VAX 11/750 used in this work was purchased in part by N.S.F. equipment Grant No. CHE-8214313.

Registry No. CH_2Li_2, 21473-62-1.

(16) (a) Laidig, W. D.; Schaefer, H. F., III. *J. Am. Chem. Soc.* **1979**, *101*, 7184. (b) Apeloig, Y.; Schleyer, P. v. R.; Binkley, J. S.; Pople, J. A. *Ibid.* **1976**, *98*, 4332.

Symmetry Aspects of Jahn–Teller Activity: Structure and Reactivity

A. Ceulemans,* D. Beyens, and L. G. Vanquickenborne*

Contribution from the Department of Chemistry, University of Leuven, 3030 Heverlee, Belgium.
Received April 13, 1983

Abstract: The Jahn–Teller theorem predicts that highly symmetrical molecules with a degenerate ground state are subject to distorting forces, acting along certain nontotally symmetric vibrational modes. These vibrations carry the nuclei over into distorted configurations, corresponding to subgroup symmetries of the parent molecular point group. The group-theoretical concepts of kernel and epikernel are of immediate relevance in this respect, since they can be shown to describe respectively the lowest subgroup attainable and the allowed intermediate subgroups. Moreover a general epikernel principle can be proposed: stationary points on a Jahn–Teller potential surface will adopt epikernel rather than kernel symmetries; higher ranking epikernels are preferred over lower ranking epikernels. By a straightforward assignment of the relevant extremal points, this principle greatly simplifies the various theoretical methods that describe potential energy surfaces near a Jahn–Teller unstable origin. In addition, the kernel and epikernel concepts offer a very concise expression of the McIver–Stanton reaction rules. The topological implications of the Jahn–Teller theorem can thus be fully explored. The present work avoids abstract terms; instead, the paper is conceived as a case study of the $T \times (t_2 + e)$ problem. Several examples relating to the structure and reactivity of metal carbonyl molecular fragments are included. In these examples the signs of the vibronic coupling constants have been obtained by a generalization of Bacci's angular overlap model treatment.

I. Introduction

The usual procedure to predict molecular shapes is to carry out a set of numerical calculations on selected geometries and to retain the one that yields an absolute minimum.[1-3] Such calculations often explore only a minute part of the Born–Oppenheimer hypersurface and may fail to elucidate the general topological structure of that surface. This structure can hardly be obtained by point-to-point calculations. Rather, what is required is an understanding of the hyperplane's geometry and its general symmetry properties.[4]

In some cases, a useful starting point is provided by the Jahn–Teller (JT) theorem, especially in its perturbational form as described by Öpik and Pryce.[5] It applies whenever the surface

(1) Elian, M.; Hoffmann, R. *Inorg. Chem.* **1975**, *14*, 1058.
(2) Burdett, J. K. *J. Chem. Soc., Faraday Trans. 2* **1974**, *70*, 1599.
(3) Burdett, J. K. "Molecular Shapes"; Wiley: New York, 1980.
(4) Pearson, R. "Symmetry Rules for Chemical Reactions"; Wiley: New York, 1976.

0002-7863/84/1506-5824$01.50/0

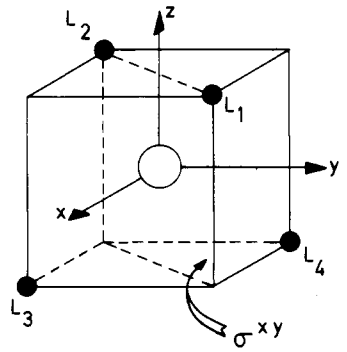

Figure 1. Cartesian frame and ligand numbering in the tetrahedral ML_4 unit. T_d subgroups will be labeled according to their orientation in this frame. As an example, in $D_{2d}{}^z$ or $C_{2v}{}^z$ the principal symmetry axis coincides with the z axis. The trigonal axis in $C_{3v}{}^{xyz}$ contains ligand 1; ligand 2 is the top ligand of $C_{3v}{}^{\bar{x}\bar{y}z}$, etc. σ_{xy} is the diagonal symmery plane which bisects the right angle between positive x and y axis. $C_s{}^{xy}$ is the associated subgroup. Similarly $\sigma_{x\bar{y}}$ contains ligands 3 and 4, etc.

is generated via symmetry-lowering distortions of a degenerate parent state in a highly symmetrical configuration.[6] Although it has been widely recognized that Jahn–Teller instability is indeed one of the key features in transition-metal stereochemistry, existing structural studies in the field apparently have not fully explored the theorem's topological implications.

In the present paper, we intend to show how symmetry principles can be used to infer the topology of the relevant adiabatic energy surfaces. The treatment will be centered on the example of the Jahn–Teller instability of a threefold degenerate state in tetrahedral metal complexes. Both the minima and the saddle points of the different surfaces will be discussed. The example is chosen because of its immediate relevance to the structure and dynamics of certain quasi-tetrahedral metal carbonyl fragments.[2,7]

II. Jahn–Teller Effect for T Terms: Symmetry Considerations

Since the symmetric product $[T_1 \times T_1] = [T_2 \times T_2] = A_1 + E + T_2$, the Jahn–Teller active vibrations for a threefold degenerate T state (T_1 or T_2) are of e and t_2 symmetry. In a tetrahedral AB_4 molecule, there is one e mode—of purely bending type—and two t_2 modes, one of which is primarily bending, while the other one is primarily stretching. Usually, interference of the two t_2 modes can be considered negligible as compared to interactions between the two quasi-degenerate bending modes. Direct experimental observation of bond length deformations in metal carbonyl fragments is entirely lacking. Therefore, the subsequent treatment will be restricted to the Jahn–Teller effect in the five-dimensional space of bending deformations. The normal coordinates will be denoted by Q_θ, Q_ϵ (for the e representation) and by Q_ξ, Q_η, Q_ζ (for the t_2 representation); the coordinate system and two characteristic vibrational coordinates are shown in Figure 1 and 2.

A. Symmetry of the Jahn–Teller Distorted Molecule. A symmetry-destroying coordinate, say Q_α (where α stands for θ, ϵ, ξ, η, or ζ), will cause a narrowing of the original group G to one of its subgroups $S \subset G$

$$G \xrightarrow{Q_\alpha} S \tag{1}$$

For a number of important point groups G, Jotham and Kettle[8] have derived which subgroups S are accessible by activating a specific JT-active vibration.

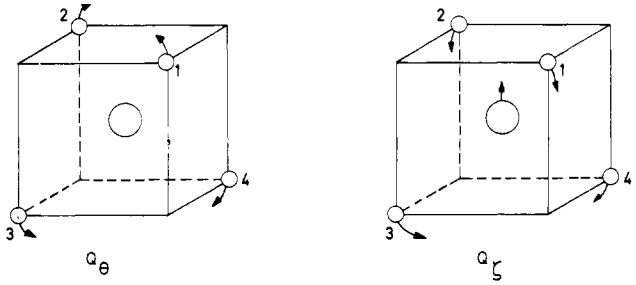

Figure 2. Representative normal modes of e type (Q_θ) and t_2 type (Q_ζ). The arrows indicate the direction of positive amplitude (see also Appendix C). Other components can be obtained by applying the standard basis relationships. If Q_θ or Q_ζ are activated, the tetrahedral symmetry is lowered to, respectively, $D_{2d}{}^z$ and $C_{2v}{}^z$.

A somewhat more general approach of the same problem is based on the group theoretical concepts of kernels and epikernels (or cokernels).[9-11] Only symmetry elements of G that leave Q_α invariant will be conserved during the distortion; all other elements will be destroyed. Therefore, *in the subgroup S, Q_α will be totally symmetric*, whereas in the parent group G, Q_α is not totally symmetric by definition: it is one of the basis vectors describing the multidimensional space of the JT-active vibrations. The representation spanned by these basis vectors will be denoted by Γ (in the T_d case, Γ can be e and/or t_2).

The *kernel* of a given representation Γ in G, denoted $K(G,\Gamma)$, is the subgroup of G, containing all symmetry elements that are represented by unit matrices in Γ. In $K(G,\Gamma)$, *all* basis functions of Γ become totally symmetric. If Γ is irreducible, the kernel is immediately obtained from character tables by collecting all symmetry elements whose characters in Γ are equal to the degeneracy of Γ. An *epikernel* of Γ in G, denoted $E(G,\Gamma)$, is a subgroup of G, containing *all* symmetry elements, for which *at least one* basis function of Γ can be chosen to be invariant.[9] Therefore, if Γ in G gives rise to Γ' in the epikernel subgroup, Γ' should be reducible and contain Γ_1 at least once. Obviously, the kernel is the trivial or the minimal epikernel.

As an example, consider the two vibrational coordinates (Q_θ, Q_ϵ), spanning the e representation of T_d. Since the character equals 2 for the identity operation and for the class of the three C_2 operations, the kernel $K(T_d,e) = D_2$. Obviously, e vibrations can destory all T_d symmetry elements, except for those belonging to D_2. Therefore, D_2 is the lowest possible symmetry attainable by e vibrations only: in D_2, both Q_θ and Q_ϵ (or any linear combination thereof) have become totally symmetric and are unable to reduce the symmetry any further.

The intermediate group D_{2d} is an epikernel $E(T_d,e)$, since the totally symmetric representation occurs only *once* in the descent in symmetry $T_d \rightarrow D_{2d}$:

$$\begin{array}{ccccc} T_d & \rightarrow & D_{2d} & \rightarrow & D_2 \\ (e) & & (a_1 + b_1) & & (a + a) \end{array} \tag{2}$$

Only one of the two e-components is invariant under the D_{2d} operations. If that particular component is activated, the symmetry is lowered to D_{2d} and not further down to D_2.

An arbitrary point in the two-dimensional (Q_θ, Q_ϵ) space is characterized by the kernel symmetry D_2 (Figure 3a). A pure Q_θ vibration corresponds to an elongation (compression) along the z axis (see Figure 2) and therefore to the epikernel symmetry $D_{2d}{}^z$ (the superscript indicates that the S_4 axis is along z). The presence of C_3 axes in T_d implies that equivalent D_{2d} structures can be generated with the S_4 axis along x or y. In the (Q_θ,Q_ϵ) plane, these equivalent structures correspond to $Q_\epsilon = -3^{1/2}Q_\theta$ for $D_{2d}{}^x$ and $Q_\epsilon = 3^{1/2}Q_\theta$ for $D_{2d}{}^y$, hence the triangular structure in Figure 3a. A point moving along the edges of this triangle cor-

(5) Öpik, U.; Pryce, M. H. L. *Proc. R. Soc. London, Ser. A* **1957**, *238A*, 425. See also: Van Vleck, J. H. *J. Chem. Phys.* **1939**, *7*, 72.
(6) For general reviews on the Jahn–Teller effect, consult: (a) Englman, R. "The Jahn–Teller Effect in Molecules and Crystals"; Wiley: New York, 1972. (b) Bersuker, I. B. *Coord. Chem. Rev.* **1975**, *14*, 357. (c) Ammeter, J. H.; Zoller, L.; Bachmann, J.; Baltzer, P.; Gamp, E.; Bucher, R.; Deiss, E. *Helv. Chim. Acta* **1981**, *64*, 1063. (d) Bersuker, I. B.; Polinger, V. Z. *Adv. Quantum Chem.* **1982**, *15*, 85–160. (e) Bersuker, I. B. "The Jahn–Teller Effect and Vibronic Interactions in Modern Chemistry"; Plenum Press: New York, 1984.
(7) Davies, B.; McNeish, A.; Poliakoff, M.; Turner, J. J. *J. Am. Chem. Soc.* **1977**, *99*, 7573.
(8) Jotham, R. W.; Kettle, S. F. A. *Inorg. Chim. Acta* **1971**, *5*, 183.
(9) Melvin, M. A. *Rev. Mod. Phys.* **1956**, *28*, 18.
(10) Ascher, E. *J. Phys. C:* **1977**, *10*, 1365.
(11) Murray-Rust, P.; Bürgi, H-B; Dunitz, J. D. *Acta Crystallogr., Sect. A* **1979**, *A35*, 703.

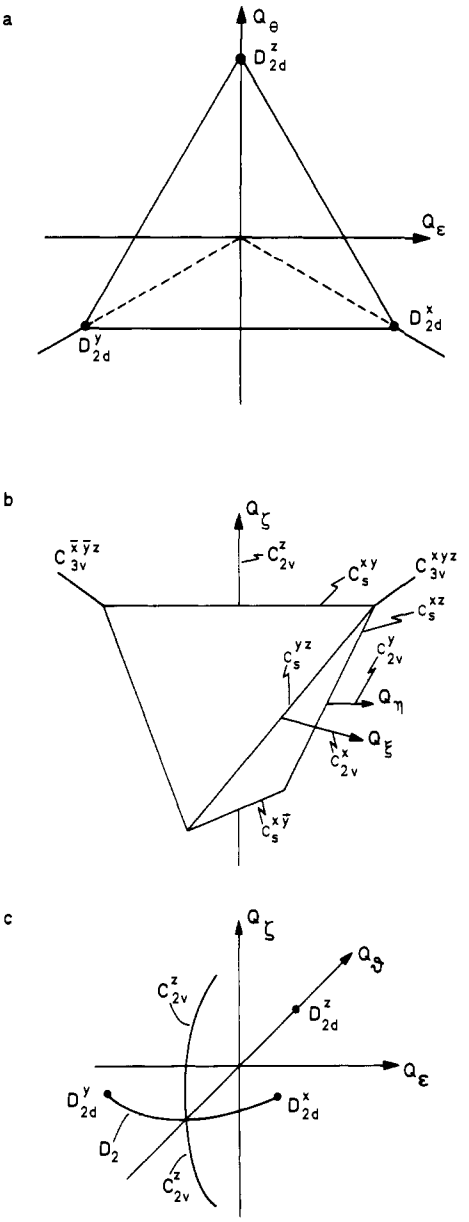

Figure 3. Perspective sections of the five-dimensional configuration space, resulting from e- and t_2-type distortions. Principal extremal points are indicated. The phase choice exemplifies the case of a $^3T_1$ electronic ground state in a tetrahedral d^8 complex (see text, eq 29). (a) Q_e space. Points on the Q_θ axis have $D_{2d}{}^z$ symmetry (cf. Figure 2). Similarly the axes $Q_\epsilon = \sqrt{3}Q_\theta$ and $Q_\epsilon = -\sqrt{3}Q_\theta$ define points with, respectively, $D_{2d}{}^y$ and $D_{2d}{}^x$ symmetries. An arbitrary point in the Q_e plane only retains the D_2 kernel symmetry. (b) Q_{t_2} space. In this case the symmetry of a configuration, represented by a spatial point, exactly corresponds to the symmetry of the site this point occupies on a tetrahedral body. As an example, activation of the three t_2 vibrations to an equal extent corresponds to a displacement along a threefold axis of the body in Figure 3b. All points on this axis have a C_{3v} site-symmetry; accordingly such a mode generates trigonally distorted molecules. (c) Combined space showing all configurations which have at least $C_2{}^z$ symmetry (cf. section VB).

responds to the epikernel D_{2d} at each vertex and at the middle of each side; everywhere else, it corresponds to the kernel D_2.

Somewhat more formally, Murray-Rust et al.[11] introduced the concept of the "homomorphic image" of a group. Since the kernel $K(G,\Gamma)$ is a normal subgroup of G, it can serve as a divisor of G, partitioning the elements of G into disjunct cosets of K. The results of the division G/K leads to the so-called factor group[12] of G by K. In the specific case where $K(T_d,e) = D_2$, the factor group G/K = T_d/D_2 corresponds to C_{3v} symmetry. Onto each element of C_{3v}, the homomorphism $T_d \rightarrow C_{3v}$ maps four different elements of T_d. In a sense then, the triangular C_{3v} structure of Figure 3a reflects the T_d symmetry in an attenuated way: it effectively incorporates the symmetry elements that were not yet considered in K. Therefore, C_{3v} is called the homomorphic image of T_d by D_2; in general, the homomorphic image of G by K is denoted $H(G,K)$.

If the homomorphism under consideration maps G onto H, the epikernel subroups of G will be mapped onto subgroups[12] of H. Therefore, the epikernels correspond to the different site symmetries of the homomorphic image. For instance, the site symmetries of the C_{3v} structure of Figure 3a are C_{3v} (origin), C_s (bisectors), and C_1 (arbitrary point), corresponding to T_d, D_{2d}, and D_2, respectively.

As a general rule, kernels and epikernels are most easily obtained upon inspection of a descent-in-symmetry sequence of the parent point group; a detailed knowledge of the actual representational matrices is not required. Descent-in-symmetry sequences[13] are exemplified in Figure 4 for the t_2 and e representations in T_d. Each first appearance of the totally symmetric representation marks an epikernel or a kernel subgroup. The kernels, epikernels, and homomorphic images are also listed in Table I. For the e representation, Figure 4 incorporates the results of eq 2. For the t_2 vibrations, the totally symmetric representation appears once in C_{2v} and C_{3v}, twice in C_s, and three times in C_1. Therefore, the kernel $K(T_d,t_2) = C_1$, and t_2 vibrations are able to destory all available symmetry. As a consequence, the ho-

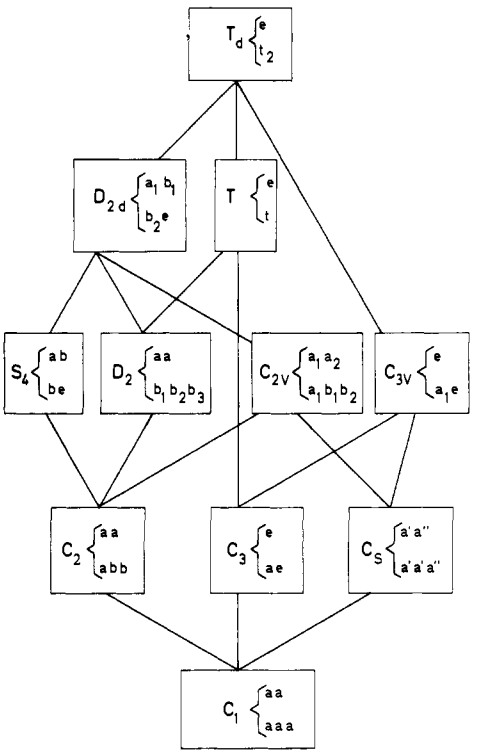

Figure 4. The genealogy of the tetrahedral point group, including the subductional chains for the e and t_2 representations.[13]

Table I. Kernel, Epikernels, and Homomorphic Image[11] for Relevant Tetrahedral Representations

Γ	$K(T_d, \Gamma)$	$E(T_d, \Gamma)^a$	$H(T_d,K)$
e	D_2	D_{2d}	C_{3v}
t_2	C_1	$C_{3v}C_{2v}C_s$	T_d
e + t_2	C_1	$D_{2d}{}^\dagger D_2{}^\dagger C_{3v}{}^\dagger C_{2v} C_2 C_s$	T_d

[a] Dagger denotes epikernels that are characteristic of e or t_2 subspaces.

(12) Baumslag, B.; Chandler, B. "Group Theory, Schaum's Outline Series"; McGraw-Hill: New York, 1968; p 122.

(13) The correlation tables corresponding to the different descent-in-symmetry chains have been listed for most symmetry groups by Wilson, Decius, and Cross in their monograph: "Molecular Vibrations"; McGraw-Hill: New York, 1955; pp 333–340.

momorphic image $H(T_d,C_1) = T_d$; it can be represented by a three-dimensional tetrahedron as in Figure 3b. The center of this body, where $Q_\xi = Q_\eta = Q_\zeta = 0$, corresponds to the undistorted tetrahedron. Activation of only one vibrational Q_{t_2} mode, say Q_ζ, lowers the site symmetry to C_{2v} (see also Figure 2); therefore all the points of the Q_ζ axis correspond to C_{2v}^z symmetry (the superscript refers to the conserved symmetry axis). Activation of the three t_2 vibrations to an equal extent generates a C_{3v} molecule—as can be verified from the site symmetry of a vertex point. Figure 4 shows that C_{2v} and C_{3v} are both "maximal epikernels", since only *one* specific Q_{t_2} combination has Γ_1 symmetry. In C_s on the other hand, two independent linear combinations of the Q_{t_2}-coordinates are invariant with respect to the remaining plane of symmetry: C_s (corresponding to the points on the edges of the tetrahedron) is a "lower ranking epikernel". An arbitrary point in the three-dimensional Q_{t_2} space corresponds to the C_1 kernel symmetry. From Figure 3b, it is also easy to visualize why C_2 cannot be an epikernel $E(T_d,t_2)$. Indeed, in a tetrahedron, any point with C_2 symmetry is situated on a site with higher C_{2v} symmetry.

Since the present treatment is concerned with the simultaneous activity of the e and t_2 modes, Table I also lists the kernels and the epikernels of the five-dimensional reducible representation (e + t_2). If the descent in symmetry generates invariances, characteristic of only one of the two vibrational types, the epikernels are marked with a dagger. For instance, from Figure 4, it is clear that D_{2d} is an (e + t_2) epikernel because of e vibrations *only*—hence the notation $D_{2d}^\dagger$. On the other hand, C_{2v} is not marked by a dagger. Although C_{2v} is an epikernel of both the t_2 and the (t_2 + e) representation, in the latter case, Γ_1 results from t_2 *and* from e. Therefore, the totally symmetric vibrations in C_{2v} can in general be linear combinations of Q_{t_2} and Q_e, and as such they are not characteristic of the t_2 surface. In this sense, C_{2v} is the maximal epikernel of the *combined* (t_2 + e) representation. In five-dimensional (Q_e, Q_{t_2}) space, only cross sections of the relevant body can be shown as Figure 3, parts a and b. Another useful subspace, shown in Figure 3c, will be discussed in the next paragraphs.

B. Symmetry of the Electronic Ground States. Within a given $\{Q_\alpha\}$ space, the symmetry lowering is such that only the kernel and the epikernel symmetries are accessible by Jahn–Teller distortions. If we first limit ourselves to the two-dimensional space of the e vibrations (Q_θ and Q_ϵ), a triply degenerate T_1 state becomes

$$\underset{(T_d)}{T_1} \rightarrow \underset{(D_{2d})}{A_2 + E} \rightarrow \underset{(D_2)}{B_1 + B_2 + B_3} \qquad (3)$$

In what follows, capital letters will be used for state symmetries, while lower case symbols designate the vibrational normal coordinates. The energy level splitting along the Q_θ axis (as shown in Figure 5) can be discussed by using a force concept approach.[14] Indeed, a molecule in a degenerate T_1 state can be said to be subject to a force

$$(T_{1t}|\partial\mathcal{H}/\partial Q_\alpha|T_{1t})_0 \neq 0 \qquad (4a)$$

corresponding to the slope of the energy curve in the high-symmetry origin; the subscript t in eq 4a stands for one of the three T_1 components and $\mathcal{H}$ symbolizes the general vibronic Hamiltonian.

It is also well-known that the sum of the forces in the origin is zero

$$\sum_t (T_{1t}|\partial\mathcal{H}/\partial Q_\alpha|T_{1t})_0 = 0 \qquad (4b)$$

where t runs over the three T_1 components. Therefore, the slope of the A_2 component is twice as steep as the slope of the E component, and A_2 will be characterized by the deepest minimum. Also, since the E component is doubly degenerate, it remains JT unstable. Within the space of the e vibrations, Q_ϵ will be activated, splitting E into $B_2 + B_3$. From Figure 3a, it can be inferred that the energy of the B_2 state drops along the Q_ϵ coordinate, until the

(14) Clinton, W. L.; Rice, B. *J. Chem. Phys.* **1959**, *30*, 542.

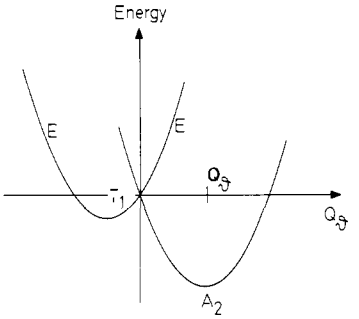

Figure 5. Potential energy surface of a T_1 state as a function of a displacement along the Q_θ coordinate, defined in Figure 2. The Q_θ distortion lowers the symmetry from T_d to D_{2d}^z (cf. Figure 3a). The T_1 level thereby splits into two components, A_2 and E. In the origin the slope of the A_2 curve is twice as large (with opposite sign) as the slope of the E curve. In consequence the A_2 curve is characterized by the deepest minimum. In this example the extremal position, Q_θ, corresponds to an elongated tetrahedron ($Q_\theta > 0$), indicating a positive linear coupling element ($V_e > 0$, see eq 12a).

D_{2d}^y structure is reached, where B_2 becomes A_2. Similarly B_3 becomes A_2 in D_{2d}^x. The three equivalent D_{2d} minima of A_2 symmetry are situated at the bottom of three intersecting paraboloids.

The energy minima of the Q_e space are thus situated in the epikernel (D_{2d}) rather than in the kernel (D_2) points. This is a manifestation of a rather general principle, which will be referred to as the "epikernel principle". A rationalization of this principle can again be obtained most readily from the force concept approach. The JT theorem itself is based on the consideration of the forces in a highly symmetric degenerate ground state; it predicts the symmetry-destroying coordinates moving the system into another point of configuration space, characterized by a lower symmetry and a nondegenerate ground state. The epikernel principle on the contrary is based on the consideration of the forces operating on the system *in these lower symmetry points*. Consider a point situated on the Q_θ axis of Figure 3a or Figure 5; the molecular ground state A_2 is in principle subject to forces parallel and perpendicular to the Q_θ axis. Now

$$(A_2|\partial\mathcal{H}/\partial Q_\epsilon|A_2) = 0 \qquad (5)$$

since Q_ϵ is a basis for the b_1 representation of D_{2d}^z, while

$$(A_2|\partial\mathcal{H}/\partial Q_\theta|A_2) \qquad (6)$$

can have any value, Q_θ being totally symmetric in D_{2d}^z. Therefore, a D_{2d} structure will experience only totally symmetric distortion forces. On the other hand, the forces on arbitrary structures in the Q_ϵ plane (D_2) will not be characterized by any type of restriction; they can adopt arbitrary values and directions.

Consequently, it is quite possible that all extremal points such as absolute minima and saddle points will be situated in epikernel points. Although it is not strictly impossible that some extremal points would also be found in the kernel symmetry, such a situation would correspond—in a sense—to the occurrence of accidental degeneracies.

For the t_2 vibrations, Table I shows that the kernel is C_1, while the epikernels are C_{3v}, C_{2v}, and C_s. One has

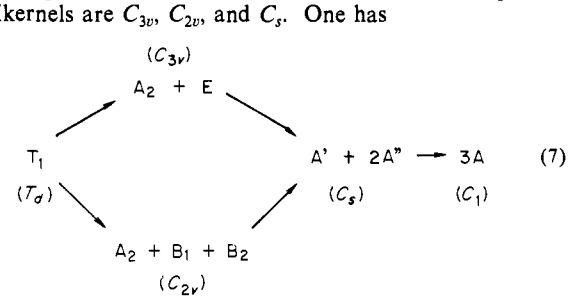

(7)

Application of the same principles reveals that extremal points of the molecular ground state can be expected for the electronically nondegenerate states of the high-symmetry epikernels C_{3v} and C_{2v}.

Indeed, Figure 4 shows that the three t_2 vibrations are $(a_1 + e)$ in C_{3v} and $(a_1 + b_1 + b_2)$ in C_{2v}; now obviously

for C_{3v}

$$(X|\partial\mathcal{H}/\partial Q_e|X) = 0$$

for C_{2v}

$$(X|\partial\mathcal{H}/\partial Q_{b_1}|X) = (X|\partial\mathcal{H}/\partial Q_{b_2}|X) = 0 \qquad (8)$$

where X stands for A_2 in C_{3v} or for any C_{2v} state. As a consequence, if the system described by X is in a C_{3v} or C_{2v} point, there can be no forces driving it into the surrounding zone of lower symmetry (see also Figure 3b). If the system is in a C_s point, there can be no forces pushing it into the surrounding C_1 zone, but there can—and in general there will—be forces driving it toward C_{3v} or C_{2v} points. Therefore, as far as the minima and the saddle points are concerned, not only are the epikernels preferred to the kernels, but the maximal epikernels are preferred to the lower ranking epikernels.

In the five-dimensional (Q_{t_2}, Q_e) space, the maximal epikernel, characteristic of the combined vibrations, is C_{2v} (Figure 4, Table I). Although C_2 and C_s points can certainly correspond to crests or valleys, the $(t_2 + e)$ extremal points are most likely to be found in C_{2v} structures.

C. Epikernel Principle. In summary, the following principle can be formulated: *Extremum points prefer epikernels to kernels; they prefer maximal epikernels to lower ranking epikernels.* More specifically, this means that as a rule stable minima are to be found with structures of maximal epikernel symmetry; there can be no forces whatsoever moving the molecule out of this symmetry, whereas in all the points of its immediate neighborhood, including the kernel points *and* the lower ranking epikernel points, the forces can, and will in general, be non-zero. Therefore, we should expect the symmetry of the stable minima to be *as high as possible*. This is a rather paradoxical conclusion, especially when compared to the Jahn–Teller theorem, which is a *symmetry reducing* theorem. In fact, there is no contradiction; both theorems are compatible, and even complementary. The Jahn–Teller theorem states what kinds of situations are unstable, whereas the epikernel principle states in what directions a stabilization is most likely to take place.

In 1894, Pierre Curie[15] formulated the following principle: *The symmetry characteristic of a phenomenon is the maximal symmetry compatible with the existence of the phenomenon.* This is certainly somewhat similar to the epikernel principle, although it was formulated long before the advent of quantum mechanics, and obviously Curie was not aware of the existence of the Jahn–Teller effect. Yet, in certain papers[10] on phase transitions in solid-state physics, the appearance of unexpected high symmetries is claimed to be related to the Curie principle. We feel, however, that the formulation of the Curie principle is too vague to be a basis for an operational rule. In order to designate the effect we have been discussing so far, we prefer to use the term "epikernel principle".

III. Öpik–Pryce Perturbational Approach

In the previous section, certain high-symmetry epikernel subgroups of T_d were shown to be of particular relevance in discussing the stable ground-state geometries. In principle, these relevant configurational subspaces can be scanned by using a number of different theoretical methods, e.g., extended Hückel theory, ligand field theory, Hartree–Fock calculations, etc. If one is especially interested in the general shape of the potential surface a cumbersome gridwise scanning of the configurational space is unnecessary and can conveniently be replaced by the Öpik–Pryce perturbational approach.[5]

Within this approach, the general vibronic Hamiltonian

$$\mathcal{H} = \sum_\alpha \left(\frac{\partial\mathcal{H}}{\partial Q_\alpha}\right)_0 Q_\alpha + \sum_\alpha\sum_\beta \frac{1}{2}\left(\frac{\partial^2\mathcal{H}}{\partial Q_\alpha \partial Q_\beta}\right)_0 Q_\alpha Q_\beta + \ldots \qquad (9)$$

can effectively be limited to the five normal coordinates discussed in the previous section: Q_θ, Q_ϵ, Q_ξ, Q_η, Q_ζ. Under these assumptions, eq 10 represents the (3×3) Hamiltonian matrix, including all quadratic terms:

$$\begin{aligned}\mathbf{H} = {} & [\tfrac{1}{2}K_e(Q_\theta^2 + Q_\epsilon^2) + \tfrac{1}{2}K_t(Q_\xi^2 + Q_\eta^2 + Q_\zeta^2)]\mathbf{J} + [V_e Q_\theta + \\ & L_e(\tfrac{1}{2}Q_\epsilon^2 - \tfrac{1}{2}Q_\theta^2) + L_t(-\tfrac{1}{2}Q_\zeta^2 + \tfrac{1}{4}Q_\zeta^2 + \tfrac{1}{4}Q_\eta^2)]\mathbf{C}_\theta + \\ & \left[V_e Q_\epsilon + L_e Q_\theta Q_\epsilon + L_t\left(-\left(\sqrt{3}/4\right)Q_\xi^2 + \left(\sqrt{3}/4\right)Q_\eta^2\right)\right]\mathbf{C}_\epsilon + \\ & \left[V_t Q_\xi + X_t Q_\eta Q_\zeta + W\left(\tfrac{1}{2}Q_\theta Q_\xi + \left(\sqrt{3}/2\right)Q_\epsilon Q_\xi\right)\right]\mathbf{C}_\xi + \\ & \left[V_t Q_\eta + X_t Q_\xi Q_\zeta + W\left(\tfrac{1}{2}Q_\theta Q_\eta - \left(\sqrt{3}/2\right)Q_\epsilon Q_\eta\right)\right]\mathbf{C}_\eta + \\ & [V_t Q_\zeta + X_t Q_\zeta Q_\eta + W Q_\zeta Q_\theta]\mathbf{C}_\zeta \qquad (10)\end{aligned}$$

The basis of this matrix representation is $|T_{1x}\rangle$, $|T_{1y}\rangle$, $|T_{1z}\rangle$ or $|T_{2\xi}\rangle$, $|T_{2\eta}\rangle$, $|T_{2\zeta}\rangle$, where the subscripts refer to Griffith's standard bases;[16] the notation is consistent with ref 17. The six parts of eq 10 correspond to the six representations and subrepresentations contained in the symmetry product $[T \times T]$. **J** is the (3×3) unit matrix, and the **C** matrices, containing the appropriate coupling coefficients,[8,17-20] are listed in Appendix A. All other quantities in eq 10 denote the typical vibronic coupling constants. Their definition can be inferred directly from the equation: K_e and K_t are the harmonic force constants; V_e and V_t are the linear JT interaction elements; W is the bilinear element arising from the coupling between t_2 and e vibrations; L_e, L_t, and X_t refer to quadratic coupling constants that result from the nontotally symmetric parts of the $e \times e$ and $t_2 \times t_2$ symmetrized direct products.

The secular equation of **H**

$$\mathbf{H}\mathbf{a}_i = \lambda_i \mathbf{a}_i \qquad (11a)$$

yields three roots $(i = 1, 2, 3)$, where $\mathbf{a}_i$ is a column vector containing one of the normalized eigenvectors of H; λ_i is the associated eigenvalue. Each root corresponds to a sheet of the adiabatic potential surface in five-dimensional space. Although trigonometric solutions of the 3×3 eigenvalue problem are available, the general expressions are highly untractable.[21] Therefore, following Öpik and Pryce,[5] we will focus our attention on the derivation of certain salient features, such as extrema and principal axes of curvature, that specifically mark the topology of the surface. Extremal points can be obtained by imposing the stationary condition

$$\bar{\mathbf{a}}_i \frac{\partial H}{\partial Q_\alpha}\mathbf{a}_i = 0$$

$$\alpha = \theta, \epsilon, \xi, \eta, \zeta; \quad \bar{\mathbf{a}}_i\mathbf{a}_i = 1 \qquad (11b)$$

upon the solutions of eq 11a. Since the Hamiltonian is quadratic in Q_α, eq 11b yields a system of five equations that are linear in the normal coordinates. Explicit formulas are given in Appendix B. These equations can be used to derive the extremal positions of Q_α, say $\boldsymbol{Q}_\alpha$, as a function of the $\mathbf{a}_i$ components. In principle the eigenvector can then be found by substituting these $\boldsymbol{Q}_\alpha$ functions in eq 11a and solving the outcoming secular equations. Again highly untractable expressions result. However in many cases the epikernel principle allows us to find $\mathbf{a}_i$ at the extrema

(15) Curie, P., Oeuvres de Pierre Curie, Gauthiers-Villars, Paris, 1908, pp 118–141.

(16) Griffith, J. S. "The Theory of Transition-Metal Ions"; Cambridge University Press: New York, 1961, Tables A5 and A16. The standard basis choice in T_d is identical with the basis choice in the isomorphous group of rotations in an octahedron.

(17) Bersuker, I. B.; Polinger, V. Z. *Phys. Lett. A* **1973**, *44A*, 495. *Sov. Phys.-JETP (Engl. Transl.)* **1974**, *39*, 1023.

(18) Griffith, J. S. "The Irreducible Tensor Method for Molecular Symmetry Groups"; Prentice-Hall: Englewood Cliffs, NJ, 1962.

(19) Ceulemans, A.; Beyens, D. *Phys. Rev. A* **1983**, *A27*, 621.

(20) In agreement with the sum rule in eq 4b, the Clebsch-Gordan coefficient matrices $C_{\Gamma\gamma}$ in Appendix A are seen to be traceless. In the origin of a JT surface several other interesting sum rules apply as well, all of which derive from the orthonormality properties of the $C_{\Gamma\gamma}$ matrices.

(21) Liehr, A. D. *Prog. Inorg. Chem.* **1962**, *3*, 281–314f; **1962**, *4*, 455–540.

immediately from symmetry considerations. Subsequently, also the energy can be calculated from eq 11a by substituting the same $\mathbf{a}_i$ coefficients as well as the Q_α values from eq 11b.

Equation 11, parts a and b, has been solved analytically by Bersuker and Polinger,[17] under the assumption that L_e, L_t, and X_t vanish, and by Bacci et al.,[22] omitting W. In a study of impurity centers in octahedral lattices, the latter authors[23] also analyzed more elaborate hamiltonians by means of numerical techniques. Additional terms, due to the effect of the totally symmetric mode and anharmonic restoring forces were thereby taken into consideration. Accounting for the a_{1g} mode is indeed indicated in octahedral symmetry, where the e_g mode involves a radial deformation, whereas the t_{2g} mode is purely bending. In tetrahedral symmetry, on the contrary, one is concerned with two quasi-degenerate bending modes. Therefore, in the present case, differential perturbations from the a_1 stretching can probably be disregarded. On the other hand, there is no a priori reason to omit any of the quadratic constants, and we will need expressions that are slightly more general than the ones obtained previously.[17,22]

IV. Extrema of the T × (t_2 + e) Equation

Using the ideas of the previous sections, we will present parametric expressions for the solutions of eq 10 and 11. First we will look for solutions of the T × (t_2 + e) problem that remain characteristic of the separate coupling T × t_2 or T × e—that is, for the subgroups marked with a dagger in Table I. In view of the epikernel principle, we will limit ourselves to the epikernels D_{2d} (for T × e) and C_{3v} (for T × t_2). These solutions are well-known[22] and can also be derived without difficulty in the framework of the present methodology. In order to find the λ_{D2d} minimum, it is sufficient to realize that one of the three equivalent eigenvectors $\mathbf{a}_{D2d}$ is determined by $a_x = a_y = 0$; $a_z = 1$. Indeed, by activating only Q_θ, the A_2 ground state (in $D_{2d}{}^z$) is given by $|T_{1z}\rangle$. Inserting these **a** components into the equations of Appendix B, one obtains the Q_α expressions

$$(Q_\theta,Q_\epsilon,Q_\xi,Q_\eta,Q_\zeta)_{D_{2d}} = \frac{V_e}{K_e + L_e}(1\ 0\ 0\ 0\ 0) \qquad (12a)$$

and, using eq 11a, it follows that

$$\lambda_{D_{2d}} = -\frac{V_e^2}{2(K_e + L_e)} \qquad (12b)$$

For C_{3v}, one similarly obtains, considering an A_2 ground state, say $a_x = a_y = a_z = 1/\sqrt{3}$

$$(Q_\theta,Q_\epsilon,Q_\xi,Q_\eta,Q_\zeta)_{C_{3v}} = \frac{2V_t}{3K_t - 4X_t}(0\ 0\ 1\ 1\ 1) \qquad (13a)$$

$$\lambda_{C_{3v}} = -\frac{2V_t^2}{3K_t - 4X_t} \qquad (13b)$$

In eq 12 and 13, we introduce only one dihedral (D_{2d}) and one trigonal (C_{3v}) point. The other equivalent and equienergetic solutions can be obtained by applying the tetrahedral symmetry operations on the coordinates of the extremum under consideration. In general, the number of equivalent configurations with a given subgroup symmetry equals the quotient of the group orders.[24] Hence there are $|T_d|/|D_{2d}| = 3$ equivalent dihedral minima (see Figure 3a) and $|T_d|/|C_{3v}| = 4$ equivalent trigonal minima (see Figure 3b).

Next in looking for solutions that are truly characteristic of the combined Hamiltonian, one has to consider the symmetry adapted state functions in the maximal epikernel group C_{2v}. If one selects $C_{2v}{}^z$, one obtains[25]

$$|A_2\rangle = |T_{1z}\rangle$$
$$|B_2\rangle = (1/\sqrt{2})[|T_{1x}\rangle + |T_{1y}\rangle]$$
$$|B_1\rangle = (1/\sqrt{2})[|T_{1x}\rangle - |T_{1y}\rangle] \qquad (14)$$

The $|T_{1z}\rangle$ function describes a nondegenerate state in $D_{2d}{}^z$ as well. As such it is not characteristic of $C_{2v}{}^z$ but rather of $D_{2d}{}^z$, containing $C_{2v}{}^z$ as a subgroup: application of the matrix equation of Appendix B leads to eq 12 as the only solution. This result is compatible with the epikernel principle, since all t_2 vibrations are nontotally symmetric in D_{2d} (see Figure 4). On the other hand, the B_1 and B_2 functions are both genuine C_{2v} components: in D_{2d}, they would correspond to the degenerate JT unstable E-state. Using the eigenvector $a_x = 1/\sqrt{2}$, $a_y = \pm 1/\sqrt{2}$, $a_z = 0$ (eq 14), one obtains

$$(Q_\theta,Q_\epsilon,Q_\xi,Q_\eta,Q_\zeta)_{C_{2v}} = \left(\frac{-V_eK_t' + 2WV_t}{2(K_e'K_t' - W^2)},0,0,0,\pm\frac{2K_e'V_t - V_eW}{2(K_e'K_t' - W^2)}\right) \qquad (15a)$$

$$\lambda_{C_{2v}} = -\frac{V_e^2K_t' + 4V_t^2K_e' - 4WV_eV_t}{8(K_e'K_t' - W^2)} \qquad (15b)$$

where

$$K_\Gamma' = K_\Gamma - \tfrac{1}{2}L_\Gamma \qquad (15c)$$

The upper sign in a_y (the B_2 state of eq 14) corresponds to the upper sign in Q_ζ (eq 15a); the B_1 state of eq 14 corresponds to the lower sign in eq 15a. There are $|T_d|/|C_{2v}| = 6$ equivalent and equienergetic solutions of C_{2v} symmetry. Within the space of the t_2 vibrations, they correspond to the middle of the six edges in Figure 3b (two on each coordinate axis); activation of the appropriate e vibration will move the system into the five-dimensional (e + t_2) space but will not otherwise affect the general picture. The two equivalent structures on both sides of say the Q_ζ axis are seen to correspond to $C_{2v}{}^z$ symmetry. From eq 15 it follows that the two equienergetic structures correspond to B_1 and B_2, respectively. In Figure 3c, these structures are represented by two points situated in the (Q_θ,Q_ζ) plane above and below the (Q_θ,Q_ϵ) plane. Four more C_{2v} points can be obtained by symmetry adaptation to $C_{2v}{}^x$ and $C_{2v}{}^y$. If $L_e = L_t = 0$ (and $K_\Gamma' = K_\Gamma$ in eq 15c), eq 15 reduces to the results obtained by Bersuker and Polinger.[17]

It is interesting to observe that the C_{2v} solution for the separate (T × t_2) problem immediately appears as a particularization of Eq 15b:

$$\lambda_{C_{2v}}{}^{Txt_2} = -\frac{V_t^2}{2K_t - L_t} \qquad (16)$$

From a comparison of eq 13b and 16, it can be concluded that under normal conditions (where L_t, $X_t << K_t$) the absolute minimum of (T × t_2) will have trigonal symmetry: $\lambda_{C_{3v}} < \lambda_{C_{2v}}{}^{Txt_2}$. For other—more exceptional—parameter values, C_{2v} could become an absolute minimum in the Q_{t_2} space. This would not be in contradiction to the epikernel principle, since both C_{2v} and C_{3v} are maximal epikernels:[10] they belong to different branches in the hierarchical chain of tetrahedral subgroups (Figure 4).

The description of stationary points corresponding to the lower ranking epikernel symmetries C_2 or C_s is more difficult, since symmetry adaptation does not project unique eigenfunctions. For instance a basis for $C_2{}^z$ might be written as follows:

$$|A\rangle = |T_{1z}\rangle$$
$$|B\rangle_1 = \alpha|T_{1x}\rangle + \sqrt{1 - \alpha^2}\,|T_{1y}\rangle \qquad (17)$$
$$|B\rangle_2 = \sqrt{1 - \alpha^2}|T_{1x}\rangle - \alpha|T_{1y}\rangle$$

The $|A\rangle$-component is not characteristic of diagonal symmetry. Hence, two possible starting eigenvectors correspond to $a_x = \alpha$,

(22) Bacci, M.; Ranfagni, A.; Fontana, M. P.; Viliani, G. *Phys. Rev. B: Solid State* **1975**, *11*, 3052.
(23) Ranfagni, A.; Mugnai, D. Bacci, M.; Montagna, M.; Pilla, O.; Viliani, G. *Phys. Rev. B: Solid State* **1979**, *20*, 5358.
(24) Fritzer, H. P. *NATO Adv. Study Inst. Ser., Ser. B*: **1979**, *43*, 179–217.

(25) In $C_{2v}{}^z$, B_1 is symmetric with respect to the σ_{xy} plane while B_2 is symmetric under σ_{xy} (see Figure 1).

Table II. Normal Mode Analysis of the Principal Extremal Points on a $T_1 \times (t_2 + e)$ JT Surface[a]

extremal point	$\|X\rangle$	$\|Y\rangle$	normal modes	noninteracting modes and associated force constants	possible transition vectors of $\|X\rangle$
D_{2d}	$\|A_2\rangle$	$\|E\rangle$	$a_1 b_1; b_2 e$	$a_1\ K_e + L_e$ $b_1\ K_e - L_e$ $b_2\ K_t + L_t$	none
C_{3v}	$\|A_2\rangle$	$\|E\rangle$	$e; a_1 e$	$a_1\ K_t - {}^4/_3 X_t$	none
C_{2v}	$\|B_1\rangle$	$\|B_2\rangle, \|A_2\rangle$	$a_1 a_2; a_1 b_1 b_2$	$a_1 \left\{ \frac{K_e' + K_t'}{2} \pm \left[\frac{(K_e' - K_t')^2}{4} + W^2 \right]^{1/2} \right.$ $b_1\ K_t + {}^1/_4 L_t + X_t$	a_2, b_2
	$\|B_2\rangle$	$\|B_1\rangle, \|A_2\rangle$	$a_1 a_2; a_1 b_1 b_2$	$a_1 \left\{ \frac{K_e' + K_t'}{2} \pm \left[\frac{(K_e' - K_t')^2}{4} + W^2 \right]^{1/2} \right.$ $b_2\ K_t + {}^1/_4 L_t + X_t$	a_2, b_1

[a] $|X\rangle$ and $|Y\rangle$ denote, respectively, ground-state and excited-state T_1-components. The subgroup representations of the e and t_2 normal modes have been obtained from Figure 4. The noninteracting modes comprise the normal modes that do not yield off-diagonal matrix elements between $|X\rangle$ and $|Y\rangle$. The final column lists the possible transition vectors of $|X\rangle$. These are nondegenerate and nontotally symmetric normal modes, that in addition are contained in the direct product of the $|X\rangle$ and $|Y\rangle$ representations (cf. text section VA).

$a_y = \pm(1 - \alpha^2)^{1/2}$, and $a_z = 0$, containing α as an unknown. Similarly, adaptation to a diagonal plane of symmetry, say C_s^{xy} (Figure 1), yields

$$|A'\rangle = (1/\sqrt{2})[|T_{1x}\rangle - |T_{1y}\rangle]$$

$$|A''\rangle_1 = \beta[|T_{1x}\rangle + |T_{1y}\rangle] + \sqrt{1 - 2\beta^2}|T_{1z}\rangle$$

$$|A''\rangle_2 = \sqrt{1/2 - \beta^2}\,[|T_{1x}\rangle + |T_{1y}\rangle] - \beta\sqrt{2}\,|T_{1z}\rangle \quad (18)$$

Again the $|A'\rangle$ component hides a higher symmetry. The C_s extremum will therefore always be antisymmetric with respect to the reflector plane. The two possible starting eigenvectors can be chosen as $a_x = a_y = \beta$, and $a_z = \pm(1 - 2\beta^2)^{1/2}$.

Both for C_2 and C_s, the coordinates of the stationary points are still (rather complicated) functions of α or β. Substitution in eq 11a leads to root-determining equations which in practice can only be solved by numerical means. Reported computer simulations[17,23] reveal that neither C_s nor C_2 points ever will become absolute minima, which is in complete agreement with the epikernel principle.

At the end of this section, it is well to stress that the validity of the reported expressions is limited to the description of the potential in the neighborhood of the tetrahedral origin. It cannot be expected to describe the whole surface of angular deformations and should therefore be restricted to typical Jahn–Teller problems.

V. Topology of the Electronic Energy Surfaces and Chemical Reactivity

In the previous sections, we have considered the symmetry and the nuclear coordinates of the extrema of the potential surface (eq 12–18); we have also discussed the symmetry and the energy of the corresponding electronic states.

Of all the conceivable extrema, however, we are only interested in the complete minima (where the energy is minimal with respect to all (five) coordinates Q_α) and in the saddle points (where the energy is minimal with respect to four Q_α and maximal with respect to one Q_α).

A. Normal Mode Analysis. In order to discover the nature of the extremum, it is useful to go back to the Öpik–Pryce procedure.[5] The Hamiltonian of eq 10 can be reexpanded around the extremal points (D_{2d}, C_{3v}, C_{2v}) and a new local force constant matrix can be constructed. Diagonalization of this matrix yields the force constants as eigenvalues and the principal axes of curvature as the associated eigenvectors. A negative force constant indicates that the cross section of the surface along the corresponding axis of curvature resembles an inverted parabolic well. Therefore, if only *one* force constant is negative, the stationary point is a saddle point. Following McIver and Stanton[26–28] the typical eigenvector of a saddle point will be called the *transition vector.*

In ref 28 Stanton and McIver have proposed a series of theorems that govern the transformation properties of the transition vector and allow to determine its symmetry species in the transition-state point group. In line with the present methodology, it is interesting to observe that these theorems on the symmetry of the transition vectors can be reformulated in a very compact way by using the kernel concept: let G be the symmetry group of the transition state and $S \subset G$ the symmetry group of the reacting molecules in the neighborhood of the transition state. Then the symmetry of the transition vector is given by the real one-dimensional representation Γ of G, defined by

$$K(G,\Gamma) = S \quad (19)$$

Indeed, the transition vector (Γ) carries the system from G into one of its subgroups S, where Γ necessarily has become totally symmetric. As an example, consider a transition-state symmetry $G = C_{2v}$. A symmetry lowering to $S = C_2$ will require a transition vector with a_2 symmetry, since a_2 is the only (non-Γ_1) representation of C_{2v} that conserves C_2

$$K(C_{2v}^z, a_2) = C_2^z \quad (20)$$

The practical significance of eq 19 is the following: *a necessary condition for an extremal point with symmetry G to be a possible saddle point on a given S–G–S pathway is that the representations of its normal modes contain the symmetry species of the transition vector* (Γ), *as determined from eq 19.* If not, the proposed pathway is topologically forbidden.

In applying this approach to a JT surface a second specific condition emerges. Indeed the *barycenter* of the three T components has to be on a positively curved surface since in a typical JT problem the totally symmetry force constants are the dominant parameters. Hence, a negative curvature in a stationary point must be compensated by a positive curvature in the excited partners at that point. As a consequence, saddle points are only expected if the ground-state $|X\rangle$ and the excited T components $|Y\rangle$ repel each other[4,5,22] due to the non-zero value of the matrix element $\langle X|\partial\mathcal{H}/\partial Q_\alpha|Y\rangle$. This leads to an additional symmetry restriction: a topologically allowed pathway on a JT surface can only have a saddle point if the symmetry species of the transition vector is contained in the direct product of the ground- and excited-state representations of the saddle point.

Both conditions prove to be valuable heuristic tools to assign possible saddle points. Table II summarizes the results of a normal mode analysis in the principal stationary points: D_{2d}, C_{3v}, and C_{2v}. Several typical features of this table are noteworthy and will be discussed in some detail.

(i) A C_{3v} structure does not contain nontotally symmetric and nondegenerate normal modes and hence, according to the

(26) McIver, J. W.; Komornicki, A. *J. Am. Chem. Soc.* **1972**, *94*, 2625.
(27) McIver, J. W.; Stanton, R. E. *J. Am. Chem. Soc.* **1972**, *94*, 8618.
(28) McIver, J. W.; Stanton, R. E. *J. Am. Chem. Soc.* **1975**, *97*, 3632.

Scheme I

$$C_{3v}^{xyz} - C_s^{xy} - C_{2v}^{z} - C_s^{xy} - C_3^{\bar{x}\bar{y}z}$$
$$|A_2\rangle \quad |A''\rangle \quad |B_2\rangle \quad |A''\rangle \quad |A_2\rangle$$

McIver–Stanton rules,[28] cannot correspond to a saddle point. This is in agreement with the topology illustrated in Figure 3b. Three equivalent pathways are seen to originate from C_{3v}. In contrast the nondegeneracy of a saddle point transition is compatible with the existence of at most two equivalent pathways: one path moving uphill from reactant to saddle point and one path moving downhill from saddle point to product.

(ii) In D_{2d} two pathways are topologically alowed, corresponding to nondegenerate b_1 and b_2 normal modes.

$$K(D_{2d},b_1) = D_2 \tag{21a}$$

$$K(D_{2d},b_2) = C_{2v} \tag{21b}$$

However the b_1 and b_2 representations are not contained in the direct product of D_{2d} ground- and excited-state components $A_2 \times E = E$. As a result these topologically allowed modes cannot be expected to give rise to negative curvature and therefore dihedral saddle points must also be rejected.

(iii) Another interesting feature is exemplified in the case of C_{2v} extremal points. If the transition vector has a_2 symmetry the C_{2v} extremum is a transition state on a C_2 path, since an a_2 vibration destroys both symmetry planes, conserving only the twofold rotation (eq 20). If the transition vector has b_1 or b_2 symmetry, the C_{2v} structure must correspond to a point on a C_s path. Moreover Table II shows that the transition vector and the transition state have opposite symmetry with respect to the two planes of symmetry: b_2 for $|B_1\rangle$ and b_1 for $|B_2\rangle$. Therefore the C_{2v} transition state will be correlated to an antisymmetric $|A''\rangle$ C_s state.

(iv) For each noninteracting mode, one expects the ground state to be on a surface with positive curvature. Table II shows parametric expressions for the corresponding force constants. In all cases, these constants are seen to be positive for a reasonable range of parameters.

In summary, group theory shows that the symmetry of a saddle point in the present case can at most be C_{2v}; lower symmetry saddle points are possible (though not derivable from group theory) for certain specific parameter combinations and at certain specific points in configuration space.

In principle, the three maximal epikernels, D_{2d}, C_{3v}, and C_{2v}, can all give rise to complete minima. Whether or not they will do so, and which one of the complete minima will be the absolute minimum, depends on the actual value of the vibronic constants figuring in the energy expressions eq 12b, 13b, and 15b.

B. Allowed vs. Forbidden Reactions. From the previous sections, it follows that three possible absolute minima should be considered: C_{3v}, D_{2d}, and C_{2v}. In some cases, several minima of different type and symmetry have been supposed to coexist;[23,29] we will limit ourselves to the simpler case where one minimum is definitely lower than the other two, and where it corresponds to a specific, experimentally observable structure. The topological routes we will consider involve transitions between equivalent minima (for instance between the four equienergetic minima in case of a C_{3v} structure). Experimentally, such processes can be observed by using isotopomers.

(i) The connections between the C_{3v} points can immediately be inferred from Figure 3b. One edge of the tetrahedron can be represented as in Scheme I. Also included in the scheme are the electronic ground states of the stationary points, as obtained from the foregoing analysis. When the character convention specified in ref 25 is used, the transition vector in the C_{2v}^z saddle point has b_1 symmetry (conservation of the σ_{xy} plane). From Table II, it follows that the C_{2v}^z ground state must be $|B_2\rangle$. This state is antisymmetric with respect to σ_{xy}, and therefore the process of Scheme I takes place on the ground-state surface: Scheme I

(29) O'Brien, M. C. M. *Phys. Rev.* **1969**, *187*, 407.

Scheme II

$$D_{2d}^{x} - C_2^{z} - C_{2v}^{z} - C_2^{z} - D_{2d}^{y}$$
$$|A_2\rangle \quad |B\rangle \quad |B_{1 \text{ or } 2}\rangle \quad |B\rangle \quad |A_2\rangle$$

Scheme III

$$C_{2v}^{z} - C_{2v}^{z} - D_{2d}^{z} - C_{2v}^{\bar{z}} - C_{2v}^{\bar{z}}$$
$$|B_2\rangle \quad |B_2\rangle \quad |A_2\rangle \quad |B_1\rangle \quad |B_1\rangle$$

represents an allowed reaction.[30] Even if the actual reaction path would partially extend into the (Q_θ,Q_ϵ) space, the conclusion on the allowed nature of the reaction would obviously not be modified.

(ii) The reaction path from one D_{2d} minimum to another one can be visualized from Figure 3a. Within the space of the e vibrations, this transition is forbidden. Indeed, as discussed in section IIB, the symmetry of the D_{2d} ground state is A_2. But in the intermediate D_2 structures, the symmetry of the ground state becomes B_1, B_2, or B_3, depending on whether the point of departure is D_{2d}^z, D_{2d}^y, or D_{2d}^x, respectively. This leads to the well-known situation of three intersecting potential wells.[6b]

In order to render the process allowed, symmetry lowering beyond D_2 is required. This symmetry lowering is only feasible through extension of Figure 3a into the t_2 space,[29] leading either to C_1 or to C_2. In view of the epikernel principle, C_2 will be preferred, and from section IV, the ground state will be $|B\rangle$. Figure 3c illustrates how the transition from D_{2d}^x to D_{2d}^y can be made possible by activation of Q_ζ: the three coordinates Q_θ, Q_ϵ, and Q_ζ are totally symmetric under C_2^z. They define a three-dimensional section of the $(Q_{t_2} + Q_e)$ space, containing all structures which have at least C_2^z symmetry. An allowed reaction path can then be represented by a curved line between D_{2d}^x and D_{2d}^y, situated above or below the (Q_θ,Q_ϵ) plane. Such a curve will cross the (Q_θ,Q_ζ) plane, which is characterized by C_{2v}^z symmetry: from section IV, the corresponding ground state will be B_1 or B_2, depending on whether Q_ζ is positive or negative. This state will be the transition state on the rearrangement path; the transition vector has a_2 symmetry (eq 20). The appropriate Scheme II is shown below. Clearly in this scheme, symmetry is being conserved and there exists an adiabatic path connecting both potential wells.

(iii) In order to discuss the C_{2v} absolute minima in the $T \times (t_2 + e)$ problem, it is useful to consider first the C_{2v} points in the $(T \times t_2)$ case. Figure 3b shows that the six equivalent C_{2v} points form the corners of an octahedron, inscribed in the tetrahedron. As opposed to the D_{2d} or C_{3v} structures, where only one reaction path had to be considered, we have to allow now for two nonequivalent routes: $C_{2v}^p \leftrightarrow C_{2v}^{\bar{p}}$, connecting opposite vertices of the octahedron, and $C_{2v}^p \leftrightarrow C_{2v}^q$, connecting adjacent vertices (p and q stand for x, y, or z; $p \neq q$). This picture remains essentially valid in the five-dimensional $(t_2 + e)$ space, where the activation of the appropriate e vibration yields an additional degree of freedom without reducing the symmetry. It will be shown in the subsequent paragraph that $C_{2v}^p \leftrightarrow C_{2v}^{\bar{p}}$ is a forbidden process, whereas $C_{2v}^p \leftrightarrow C_{2v}^q$ is an allowed process.

C. Rearrangements of the C_{2v} Structures. (i) Consider first the rearrangement $C_{2v}^p \leftrightarrow C_{2v}^{\bar{p}}$, *when all the symmetry elements are conserved*; within the t_2 space (Figure 3b), this corresponds to a movement of the configurational point along one of the coordinate axes, say Q_ζ (for C_{2v}^z), and passing through the origin of the figure (T_d symmetry). However, each point in Figure 3b corresponds to a two-dimensional (Q_θ,Q_ϵ) plane in the $(t_2 + e)$ space. Therefore, if extension into the Q_e space is allowed—while conserving the C_{2v} symmetry—the origin of Figure 3b will in general correspond to D_{2d} symmetry. In the example of C_{2v}^z, the appropriate e vibrational coordinate is Q_θ, and the reaction actually

(30) The normal mode analysis of T_2 ground-state components yields similar conclusions. As an example the C_{2v} transition state is now shown to have the same symmetry as the C_s path transition vector: b_1 for $|B_1\rangle$ and b_2 for $|B_2\rangle$. Hence, the transition state correlates with $|A'\rangle$ C_s states. But now the C_{3v} ground-state symmetry also has changed from $|A_2\rangle$ to $|A_1\rangle$, and Scheme I remains an electronically allowed process.

Scheme IV

$$C_{2v}{}^{z}\text{—}C_{2}{}^{z}\text{—}D_{2d}{}^{z}\text{—}C_{2}{}^{z}\text{—}C_{2v}{}^{\bar{z}}$$
$$|B_2\rangle \quad |B\rangle \quad |A_2\rangle \quad |B\rangle \quad |B_1\rangle$$

Scheme V

$$C_{2v}{}^{z}\text{—}C_{2}{}^{z}\text{—}D_{2d}{}^{y\text{ or }x}\text{—}C_{2}{}^{z}\text{—}C_{2v}{}^{\bar{z}}$$
$$|B_2\rangle \quad |B\rangle \quad |A_2\rangle \quad |B\rangle \quad |B_1\rangle$$

takes place in the two-dimensional (Q_ζ,Q_θ) space (Figure 3C); it can be represented by Scheme III. It has been shown in section IV that the electronic ground states of $C_{2v}{}^{z}$ are $|B_1\rangle$ or $|B_2\rangle$, depending on the sign of Q_ζ. Therefore, in any case the ground-state symmetry will be different on both sides of the transition state: a transition vector cannot be properly defined and the reaction is forbidden. The same conclusion can also be found by realizing that $|B_1\rangle$ and $|B_2\rangle$ cross in the excited degenerate $|E\rangle$ state of $D_{2d}{}^{z}$; they are obviously not connected to the D_{2d} ground-state surface (which has A_2 symmetry).

(ii) The forbidden character of he $C_{2v}{}^{p} \leftrightarrow C_{2v}{}^{\bar{p}}$ reaction is maintained even if the symmetry of the reaction path is lowered to C_s. Indeed, for both mirror planes of C_{2v}, the B_1 and B_2 states are characterized by opposite behavior, and a ground-state correlation is impossible.

(iii) Since B_1 and B_2 have the same character (−1) for $C_2{}^{z}$, they both give rise to an antisymmetric $|B\rangle$ state, and therefore a $C_2{}^{z}$ path should be a more likely route for an allowed reaction; this path should be situated entirely in the three-dimensional subspace of Figure 3c and the transition state must be situated in the (Q_θ,Q_ϵ) plane, more specifically in one of the epikernel D_{2d} points. There are two possibilities and either Scheme IV or Scheme V applies. Since A_2 is symmetric under $C_2{}^{z}$ in $D_{2d}{}^{z}$, whereas B is antisymmetric, the ground state of the $C_{2v}{}^{z}$ structure is necessarily connected to an excited state of $D_{2d}{}^{z}$ and not to its $|A_2\rangle$ ground state: the reaction is electronically forbidden. Moreover according to eq 21 Scheme IV represents a topologically forbidden pathway. In Scheme V, the reaction is electronically allowed, since A_2 is antisymmetric under $C_2{}^{z}$ in $D_{2d}{}^{y\text{ or }x}$. But the McIver–Stanton rules prevent the $D_{2d}{}^{y\text{ or }x}$ structures from being saddle points on a $C_2{}^{z}$ route: indeed the D_{2d} group does not contain a nondegenerate representation Γ for which $K(D_{2d}{}^{y\text{ or }x},\Gamma) = C_2{}^{z}$. The absence of dihedral saddle points is in agreement with the conclusions of Table II.

(iv) The only remaining possibility for the $C_{2v}{}^{p} \leftrightarrow C_{2v}{}^{\bar{p}}$ reaction is to proceed via an asymmetric C_1 path. In that case, the epikernel principle requires the saddle point to be C_2 or C_s. However, the mirror plane or the rotation axis cannot be one of the symmetry elements of the $C_{2v}{}^{p}$ structure. Indeed, if it were, the transition vector would necessarily be antisymmetric with respect to that particular symmetry operation (it would for instance be a vector perpendicular to the mirror plane). But the McIver–Stanton rules[28] require that the transition vector be symmetric with respect to any symmetry operation that leaves either reactants or products unchanged. Therefore, the saddle point can only be characterized by a C_2 or a mirror plane that does not belong to the $C_{2v}{}^{p}$ structure itself. As a specific example, a $C_s{}^{xz}$ plane might conceivable be a saddle point for the $C_{2v}{}^{z} \leftrightarrow C_{2v}{}^{\bar{z}}$ rearrangement (Figure 3b). But obviously any $C_{2v}{}^{z} - C_s{}^{xz}$ valley should be equivalent to a corresponding $C_s{}^{xz} - C_{2v}{}^{x}$ valley; therefore, the C_1 path connects $C_{2v}{}^{p}$ to $C_{2v}{}^{q}$, not to $C_{2v}{}^{\bar{p}}$. The situation is also illustrated in Figure 6, where the C_1 path is projected in the (Q_ζ,Q_ξ) plane. A transition from $C_{2v}{}^{z} \leftrightarrow C_{2v}{}^{\bar{z}}$ cannot cross $C_s{}^{xz}$ without at the same time crossing $C_s{}^{x\bar{z}}$. This means that the path has two saddle points; the minimum in between is $C_{2v}{}^{x}$.

(v) From the previous analysis, it follows already that the $C_{2v}{}^{p} \leftrightarrow C_{2v}{}^{q}$ rearrangement is an allowed process, as is shown in Scheme VI. Within the t_2 space the pathway can be visualized by the movement of a configurational point along one of the edges of the inscribed octahedron (Figure 3b).

The electronic process in Scheme VI is of course allowed, due to the extreme symmetry lowering in the intermediate points.

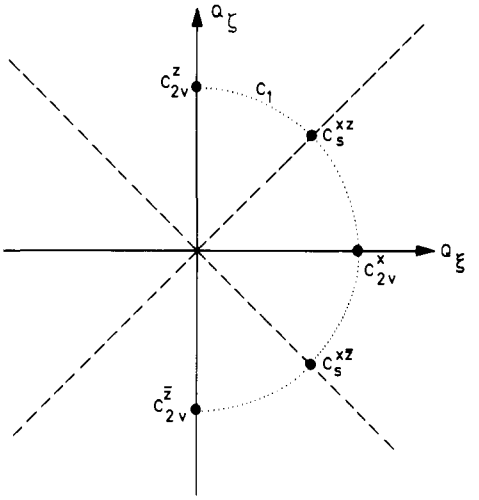

Figure 6. Cross section of the Q_{t_2} configurational space, shown in Figure 3b. Solid coordinate axes (—) represent C_{2v} points. Antipodal structures such as $C_{2v}{}^{z}$ and $C_{2v}{}^{\bar{z}}$ are on opposite sides of the T_d center (cf. eq 15a). Broken lines (---) symbolize structures that only have C_s symmetry. The dotted line (···) represents a C_1 pathway between antipodal C_{2v} structures. If this route contains one saddle point, say on $C_s{}^{xz}$, it will for obvious topological reasons also cross a second equivalent saddle pont on $C_s{}^{x\bar{z}}$. In between lies another C_{2v} minimum in casu $C_{2v}{}^{x}$. *Therefore the interchange of antipodal isotopomers necessarily proceeds via an adjacent isotopomer.* These conclusions remain valid if the C_1 path is extended into the five-dimensional $(t_2 + e)$ space (cf. Scheme VI).

Scheme VI

$$C_{2v}{}^{z}\text{———}C_1\text{—}C_s{}^{xz}\text{—}C_1\text{———}C_{2v}{}^{x}$$
$$|B_{1\text{ or }2}\rangle \quad |A\rangle \quad |A''\rangle \quad |A\rangle \quad |B_{1\text{ or }2}\rangle$$

In conclusion, as a direct result of electronic and topological selection rules, the minimal energy path connecting two antipodal C_{2v} structures involves two consecutive steps between adjacent C_{2v} structures. A striking experimental confirmation of these results will be presented in section VIIB.

VI. Evaluation of Reduced Matrix Elements for JT Coupling

Before one can compare the general conclusions of the previous sections with experiment, it will be necessary to have a semiquantitative idea on the relative magnitude of the different vibronic constants in the interaction Hamiltonian.

In an interesting series of papers, Bacci[31,32] has used ligand field theory—in its angular overlap (AOM) version[33]—to obtain a quick and simple parametrization method for certain JT coupling constants.[34] According to AOM, the one-electron ligand field matrix elements are given by

$$H_{ij} = (d_i|\mathcal{H}|d_j) = \sum_{L} \sum_{m=1}^{5} T_{im}{}^{L}\, T_{jm}{}^{L}\, H_{mm}{}^{L} \qquad (22)$$

where T^L is the AOM rotation matrix for ligand L, depending on the spherical polar coordinates of L; m runs over the five d orbitals and for any given ligand $H_{11} = \sigma$, $H_{22} = H_{33} = \pi$, $H_{44} = H_{55} = 0$.

The characteristic AOM parameters σ and π should of course depend on the metal–ligand distance R, but explicit radial functions describing this dependence are beyong the scope of the model proper. Equation 22 is therefore ideally suited for the description of purely bending modes (e and t_2) that leave the metal–ligand bond distances unchanged. As shown in eq 9 and 10, the vibronic constants K, L, V, etc. are obtained from integrals over the operators $(\partial\mathcal{H}/\partial Q_\alpha)$. Since the Q_α's describe specific angular displacements of the ligands, the operators $(\partial\mathcal{H}/\partial Q_\alpha)$

(31) Bacci, M. *Chem. Phys. Lett.* **1978**, *58*, 537.
(32) Bacci, M. *Chem. Phys.* **1979**, *40*, 237.
(33) Schäffer, C. E.; Jørgensen, C. K. *Mol. Phys.* **1965**, *9*, 401.
(34) See also for a similar treatment of f electrons: Warren, K. D. *Inorg. Chem.* **1982**, *21*, 3467.

should be expressible in terms of the individual ligand operators $(\partial\mathcal{H}/\partial\varphi_L)$ and $(\partial\mathcal{H}/\partial\theta_L)$. The use of spherical polar coordinates necessitates special care in the action of the relevant differential operators. As Bacci's papers do not discuss this point in any detail, a few remarks are necessary in order to extend the use of AOM to the calculation of general vibronic constants. The infinitesimal displacements of a point ligand L are described by the nabla in spherical coordinates

$$\nabla_L = \left(\frac{\partial}{\partial R_L}, \frac{1}{R_L}\frac{\partial}{\partial\theta_L}, \frac{1}{R_L \sin\theta_L}\frac{\partial}{\partial\varphi_L}\right) \tag{23}$$

where the first component refers to radial changes, the second to a displacement along a meridian, the third to a change in longitude along a parallel. Let **Q** be the row matrix of normal modes and **q** the row matrix of individual ligand angular displacements. Then it is possible to define a unitary matrix such that

$$d\mathbf{Q} = d\mathbf{q}\cdot\mathbf{U} \tag{24}$$

The elements of **U** are denoted $U_{L1,\alpha}$ where the row index designates the ligand L and the nabla component 1 indicating the role of each specific $\nabla_L{}^1$ component in d**Q**; the column index α refers to the symmetry of the normal mode. For the angular displacements of a tetracoordinated T_d molecule, the quantities in eq 24 are given explicitly in Appendix C. Phase conventions are in agreement with ref 31, 32.

The linear and second-order differential operators are given by

$$\partial/\partial Q_\alpha = \sum_{L1} U_{L1,\alpha}\nabla_L{}^1 \tag{25a}$$

$$\frac{\partial^2}{\partial Q_\alpha \partial Q_\beta} = \sum_{L1}\sum_{L'1'} U_{L1,\alpha}U_{L'1',\beta}(\nabla\nabla)_{LL'}{}^{11'} \tag{25b}$$

Since the AOM potential is additive in the ligands, it seems reasonable to neglect the interligand terms ($L \neq L'$) in eq 25b. The intraligand term $(\nabla\nabla)_{LL}{}^{11'}$ is not an ordinary product of linear differential operators, but it corresponds to a tensor, as given by Stone:[35]

$$\nabla\nabla_{LL} = \begin{bmatrix} \frac{\partial^2}{\partial R_L{}^2} & \frac{\partial}{\partial R_L}\frac{1}{R_L}\frac{\partial}{\partial\theta_L} & \frac{\partial}{\partial R_L}\frac{1}{R_L \sin\theta_L}\frac{\partial}{\partial\varphi_L} \\ \frac{\partial}{\partial R_L}\frac{1}{R_L}\frac{\partial}{\partial\theta_L} & \frac{1}{R_L}\frac{\partial}{\partial R_L} + \frac{1}{R_L{}^2}\frac{\partial^2}{\partial\theta_L{}^2} & \frac{1}{R_L{}^2}\frac{\partial}{\partial\theta_L}\frac{1}{\sin\theta_L}\frac{\partial}{\partial\varphi_L} \\ \frac{\partial}{\partial R_L}\frac{1}{R_L \sin\theta_L}\frac{\partial}{\partial\varphi_L} & \frac{1}{R_L{}^2}\frac{\partial}{\partial\theta_L}\frac{1}{\sin\theta_L}\frac{\partial}{\partial\varphi_L} & \frac{1}{R_L}\frac{\partial}{\partial R_L} + \frac{1}{R_L{}^2 \sin^2\theta_L}\frac{\partial^2}{\partial\varphi_L{}^2} + \frac{\cot\theta_L}{R_L{}^2}\frac{\partial}{\partial\theta_L} \end{bmatrix} \tag{26}$$

This tensor is symmetrical and its trace equals the Laplacian ∇^2. The surface operator applicable to purely angular motions can be obtained from eq 26 by imposing a constant value of R_L.

Using these expressions, the actual calculations can be carried out without difficulty. Table III collects all the required linear and quadratic coupling elements for the t_2 orbital basis. More complete tables of the linear terms can be found from the literature.[32] In this way, the different constants of eq 10 (K, V, L, X, and W) can all be expressed in terms of the ligand field parameters σ and π.

It is well to stress that the linear terms satisfy the symmetry requirements of the Clebsch-Gordan coefficients (Appendix A), while the quadratic terms of Table III can be seen to obey the higher order symmetry restrictions, derived by Englman.[6a]

(35) Stone, A. J. *Mol. Phys.* **1980**, *41*, 1339.

Table III. Relevant Linear and Quadratic Jahn-Teller Coupling Matrix Elements for the Tetrahedral Bending Modes in the d Orbital Base of the Three t_2 Orbitals, ξ, η, ζ[a]

JT-active bending mode	non-zero JT matrix elements
e	$\langle\xi\|\frac{\partial H}{\partial Q_\theta}\|\xi\rangle = \langle\eta\|\frac{\partial H}{\partial Q_\theta}\|\eta\rangle = \frac{2\sqrt{2}}{3R}(\sigma - \pi/3)$ $\langle\xi\|\frac{\partial H}{\partial Q_\epsilon}\|\xi\rangle = -\langle\eta\|\frac{\partial H}{\partial Q_\epsilon}\|\eta\rangle = -\frac{2\sqrt{6}}{3R}(\sigma - \pi/3)$ $\langle\zeta\|\frac{\partial H}{\partial Q_\theta}\|\zeta\rangle = -\frac{4\sqrt{2}}{3R}(\sigma - \pi/3)$
t_2	$\langle\xi\|\frac{\partial H}{\partial Q_\zeta}\|\eta\rangle = \langle\xi\|\frac{\partial H}{\partial Q_\eta}\|\zeta\rangle = \langle\eta\|\frac{\partial H}{\partial Q_\xi}\|\zeta\rangle = -\frac{2\sqrt{2}}{3R}(\sigma - 7\pi/3)$
$t_2 \times t_2$	$\langle\xi\|\frac{\partial^2 H}{\partial Q_\eta{}^2}\|\xi\rangle = \langle\eta\|\frac{\partial^2 H}{\partial Q_\zeta{}^2}\|\eta\rangle = \langle\zeta\|\frac{\partial^2 H}{\partial Q_\xi{}^2}\|\zeta\rangle = -\frac{7\sigma}{3R^2} + \frac{31\pi}{9R^2}$ $\langle\xi\|\frac{\partial^2 H}{\partial Q_\zeta{}^2}\|\xi\rangle = \langle\eta\|\frac{\partial^2 H}{\partial Q_\xi{}^2}\|\eta\rangle = \langle\zeta\|\frac{\partial^2 H}{\partial Q_\eta{}^2}\|\zeta\rangle = -\frac{7\sigma}{3R^2} + \frac{31\pi}{9R^2}$ $\langle\xi\|\frac{\partial^2 H}{\partial Q_\xi{}^2}\|\xi\rangle = \langle\eta\|\frac{\partial^2 H}{\partial Q_\eta{}^2}\|\eta\rangle = \langle\zeta\|\frac{\partial^2 H}{\partial Q_\zeta{}^2}\|\zeta\rangle = \frac{2\sigma}{3R^2} - \frac{14\pi}{9R^2}$ $\langle\xi\|\frac{\partial^2 H}{\partial Q_\xi \partial Q_\eta}\|\eta\rangle = \langle\eta\|\frac{\partial^2 H}{\partial Q_\eta \partial Q_\zeta}\|\zeta\rangle = \langle\zeta\|\frac{\partial^2 H}{\partial Q_\zeta \partial Q_\xi}\|\xi\rangle = \frac{7\sigma}{6R^2} - \frac{7\pi}{18R^2}$
e × e	$\langle\xi\|\frac{\partial^2 H}{\partial Q_\theta{}^2}\|\xi\rangle = \langle\eta\|\frac{\partial^2 H}{\partial Q_\theta{}^2}\|\eta\rangle = -\frac{7\sigma}{3R^2} + \frac{31\pi}{9R^2}$ $\langle\xi\|\frac{\partial^2 H}{\partial Q_\epsilon{}^2}\|\xi\rangle = \langle\eta\|\frac{\partial^2 H}{\partial Q_\epsilon{}^2}\|\eta\rangle = -\frac{\sigma}{3R^2} + \frac{\pi}{9R^2}$ $\langle\xi\|\frac{\partial^2 H}{\partial Q_\theta \partial Q_\epsilon}\|\xi\rangle = -\langle\eta\|\frac{\partial^2 H}{\partial Q_\theta \partial Q_\epsilon}\|\eta\rangle = -\frac{\sqrt{3}\sigma}{R^2} + \frac{5\pi}{\sqrt{3}R^2}$ $\langle\zeta\|\frac{\partial^2 H}{\partial Q_\theta{}^2}\|\zeta\rangle = \frac{2\sigma}{3R^2} - \frac{14\pi}{9R^2}$ $\langle\zeta\|\frac{\partial^2 H}{\partial Q_\epsilon{}^2}\|\zeta\rangle = -\frac{10\sigma}{3R^2} + \frac{46\pi}{9R^2}$
e × t_2	$\langle\xi\|\frac{\partial^2 H}{\partial Q_\theta \partial Q_\eta}\|\zeta\rangle = \langle\eta\|\frac{\partial^2 H}{\partial Q_\theta \partial Q_\xi}\|\zeta\rangle = -\frac{7\sigma}{6R^2} + \frac{25\pi}{18R^2}$ $\langle\xi\|\frac{\partial^2 H}{\partial Q_\epsilon \partial Q_\eta}\|\zeta\rangle = -\langle\eta\|\frac{\partial^2 H}{\partial Q_\epsilon \partial Q_\xi}\|\zeta\rangle = -\frac{7\sigma}{2\sqrt{3}R^2} + \frac{25\pi}{6\sqrt{3}R^2}$ $\langle\eta\|\frac{\partial^2 H}{\partial Q_\theta \partial Q_\zeta}\|\xi\rangle = \frac{7\sigma}{3R^2} - \frac{25\pi}{9R^2}$

[a] R refers to the metal-to-ligand distance and σ and π are the AOM parameters. The linear matrix elements are taken from ref 32.

VII. Comparison with Experiment

A. Static Geometry. As far as the static JT effect is concerned, the foregoing analysis can be summarized in the following way: in the absence of quadratic vibronic coupling absolute minima can only be of D_{2d} or C_{3v} symmetry. If quadratic coupling is

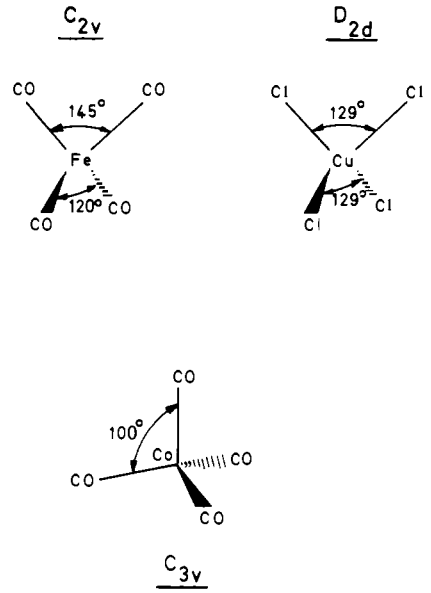

Figure 7. Examples of the static JT effect for T terms: $Fe(CO)_4$ (d^8) retains C_{2v} symmetry.[7] $CuCl_4^{2-}$ (d^9) exhibits a compressed tetrahedral structure with D_{2d} symmetry.[46] $Co(CO)_4$ (d^9) is reported[39a] to adopt an umbrella-like trigonal structure (C_{3v}) with an opening angle of circa 100°.

introduced (L, X, W in eq 10 are non-zero), C_{2v} absolute minima might arise.

More specifically, if $L_e > 0$, the D_{2d} minimum of eq 12b will become less stable than in the linear approximation. Similarly, eq 13b shows that negative X_t values tend to destabilize the trigonal minimum. The C_{2v} extremum is influenced in a somewhat more complex way. If both L_e and L_t are positive, and thus $K'_T < K_T$ (eq 15c), the denominator of eq 15b becomes quite small, resulting in a marked stabilization of the C_{2v} structure. This effect will be reinforced if WV_eV_t is negative and if the bilinear ($t_2 \times e$) coupling element W is large.

Since the sign of the distortion coordinates in eq 12a, 13a, and 15a is determined by the same parameters, predictions of the equilibrium structures become also possible.

All these relative predictions will be looked upon as the minimal empirical relevance of the AOM estimated values of the vibronic constants. They should provide a general understanding of the JT mechanism in a multidimensional problem, without requiring a gridwise search of the surface.

Certain tetrahedral members of the carbonyl fragment series provide a test case of our treatment. The best studied example[36,37] is the d^8 system $Fe(CO)_4$; its structure has been determined from a detailed analysis of the IR spectrum in the CO-stretching region;[38] it is shown in Figure 7. The fragment clearly has C_{2v} symmetry. The structure of the related d^9 systems, $Fe(CO)_4^-$ ion, and the isoelectronic $Co(CO)_4$ fragment has not been determined equally unambiguously; the symmetry does not appear to be C_{2v}, however, but rather D_{2d} or C_{3v}, possibly coexistent.[39,40]

Apparently for a d^8 system, such as $Fe(CO)_4$, one expects the parent tetrahedral state to be a $^3T_1$, based on the configuration $e^4t_2^4$. MCD measurements provide evidence that $Fe(CO)_4$ is paramagnetic, in agreement with a triplet ground-state assignment.[41] Other concurrent arguments regarding the triplet nature of the ground state can be obtained from theoretical calculations. Burdett was able to rationalize the observed C_{2v} geometry on the basis of an AOM treatment, assuming a high-spin ground state.[2] In fact, typical tetracoordinated low-spin d^8 complexes invariably adopt a square-planar geometry. Recently, the triplet character of the $Fe(CO)_4$ ground state was also confirmed by an ab initio calculation, using observed bond angles.[42] Clearly the $^3T_1(e^4t_2^4)$ ground state specification characterizes $Fe(CO)_4$ as a typical JT distorted molecule. Also the extent of the distortion is well within the range of a vibronic coupling mechanism. As an example, in $CuCl_4^{2-}$—which is characterized by a much weaker ligand field—two of the Cl–Cu–Cl angles are opened up to 129° (see Figure 7), in qualitative agreement with Bacci's vibronic analysis, based on the AOM.[32] The basic assumptions underlying the d orbital treatment set forth in section VI thus certainly are validated.[43]

Let the open shell part of the $^3T_1(d^8)$ and the $^2T_2(d^9)$ states be represented by eq 27, corresponding to t_2^4 and t_2^5 configurations, respectively:

$$\begin{aligned} |^3T_{1x}\rangle &= |\xi^2\eta\zeta| \\ |^3T_{1y}\rangle &= -|\xi\eta^2\zeta| \\ |^3T_{1z}\rangle &= |\xi\eta\zeta^2| \\ |^2T_{2\xi}\rangle &= |\xi\eta^2\zeta^2| \\ |^2T_{2\eta}\rangle &= |\xi^2\eta\zeta^2| \\ |^2T_{2\zeta}\rangle &= |\xi^2\eta^2\zeta| \end{aligned} \tag{27}$$

The single determinant functions consist of a half-filled shell subsystem (which cannot contribute to JT activity[44]) and one t_2 electron (t^4) or one t_2 hole (t^5). The JT constants as defined in eq 10 can now readily be obtained from the corresponding $^3T_1$ or $^2T_2$ matrix elements. In the d^8 case one has for instance

$$V_e = -\left\langle {}^3T_{1z}\left|\frac{\partial\mathcal{H}}{\partial Q_\theta}\right|{}^3T_{1z}\right\rangle,\ L_e = \left\langle {}^3T_{1x}\left|\frac{\partial^2\mathcal{H}}{\partial Q_\epsilon^2} - \frac{\partial^2\mathcal{H}}{\partial Q_\theta^2}\right|{}^3T_{1x}\right\rangle, \text{ etc.} \tag{28}$$

Combining these expressions with the one-electron matrix elements in Table III finally yields

$$\begin{aligned} V_e &= \pm\frac{4\sqrt{2}}{3R}\left(\sigma - \frac{\pi}{3}\right) \\ V_t &= \pm\frac{2\sqrt{2}}{3R}\left(\sigma - \frac{7\pi}{3}\right) \\ L_e &= \pm\frac{2}{R^2}\left(\sigma - \frac{5\pi}{3}\right) = L_t \\ X_t &= \mp\frac{7}{6R^2}\left(\sigma - \frac{\pi}{3}\right) \\ W &= \mp\frac{7}{3R^2}\left(\sigma - \frac{25\pi}{21}\right) \end{aligned} \tag{29}$$

where the upper signs refer to $^3T_1$, the lower signs to $^2T_2$. The σ parameter is certainly positive, and for a π acceptor ligand such as CO, it is generally assumed that $\pi < 0$. Hence, for d^8 systems V_e, V_t, L_e, and L_t are predicted to be positive, while X_t and W will be negative. These are precisely the sign combinations favoring the experimentally observed C_{2v} structure of $Fe(CO)_4$. The opposite predictions for d^9 systems are in agreement with the C_{3v} and/or D_{2d} symmetry suggested for $Fe(CO)_4^-$ and $Co(CO)_4$. Also,

(36) Poliakoff, M.; Turner, J. J. In "Chemical and Biochemical Applications of Lasers"; Moore, C. B., Ed.; Academic Press: New York, 1980; Vol. 5, pp 175–216.
(37) Poliakoff, M. *Chem. Soc. Rev.* **1978**, *7*, 527.
(38) Poliakoff, M.; Turner, J. J. *J. Chem. Soc., Dalton Trans.* **1974**, 2276.
(39) (a) Crichton, O.; Poliakoff, M.; Rest, A. J.; Turner, J. J. *J. Chem. Soc., Dalton Trans.* **1973**, 1321. (b) Hanlan, L. A.; Huber, H.; Kündig, E. P.; McGarvey, B. R.; Ozin, G. A. *J. Am. Chem. Soc.* **1975**, *97*, 7054.
(40) Breeze, P. A.; Burdett, J. K.; Turner, J. J. *Inorg. Chem.* **1981**, *20*, 3369.
(41) Barton, T. J.; Grinter, R.; Thomson, A. J.; Davies, B.; Poliakoff, M. *J. Chem. Soc., Chem. Commun.* **1977**, 841.
(42) Veillard, A. *Nouv. J. Chim.* **1981**, *5*, 599. Personal communication.
(43) Note that in the vicinity of a tetrahedral origin s orbital participation is unlikely to be very large since s–d mixing is strictly forbidden in T_d symmetry. Admittedly d–p mixing can occur, but since all three t_2 orbitals will be stabilized approximately to the same extent, we do not expect the proposed energetics to be invalidated.
(44) Ceulemans, A.; Beyens, D.; Vanquickenborne, L. G. *J. Am. Chem. Soc.* **1982**, *104*, 2988.

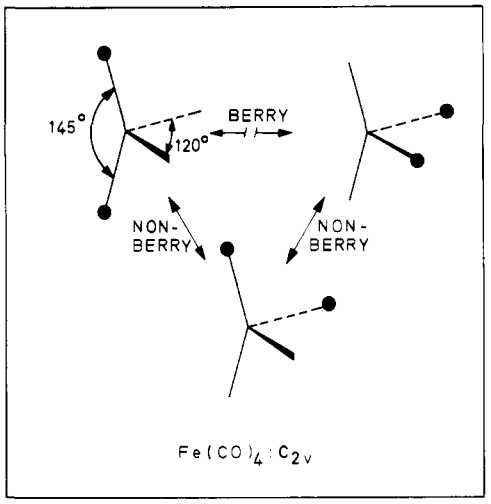

Figure 8. Detectable isomerization modes between the three possible isotopomers of $Fe(CO)_2(^{13}C^{18}O)_2$. The black circles represent $^{13}C^{18}O$. The so-called Berry process corresponds to the concerted exchange of axial sites (at an angle of 145°) and equatorial sites (at 120°). The incomplete pseudo-rotation is referred to as the non-Berry mode. Only the latter mode can be induced by IR laser light.[37]

going beyond the class of the metal carbonyl compounds, and considering $CuCl_4^{2-}$, a d^9 system where $\pi > 0$, the signs of eq 29 will not be changed, and from a combination of eq 12b, 13b, and 29, one predicts a D_{2d} ground state—again in agreement with experiment.[32,45,46]

As far as the sense of the relevant distortion is concerned (compression, elongation, etc.) the most detailed data can apparently be derived from an IR analysis, based on the band intensity/frequency factored force field method.[47] For $Fe(CO)_4$, the thus obtained information on the C–M–C bond angles shows that the fragment shape approximately resembles a flattened tetrahedron[38] (see also Figure 7). Choosing a $C_{2v}{}^z$ symmetry alignment, the observed bond angles therefore correspond to $Q_\theta < 0$ (tetragonal component of the distortion). From eq 15a, one will verify that negative Q_θ values imply $V_e > 0$ and $WV_t < 0$; eq 29 shows that these conditions are indeed satisfied for a d^8 system.

A $C_{3v}{}^{xyz}$ symmetry fitting of the IR spectrum[40] of the d^9 system $Co(CO)_4$ leads to negative values for Q_ξ, Q_η, and Q_ζ and hence to $V_t < 0$ (eq 13a). Again this observation is in agreement with the AOM predictions of eq 29.

B. Dynamic Behavior. Rearrangements on a JT surface, as described in the topological schemes of the previous section, can only be observed by using isotope labeling.[48]

Remarkably extensive studies of isotopically enriched $Fe(CO)_4$ fragments have been carried out by Poliakoff and Turner.[7,37,49] They revealed the occurrence of stereospecific rearrangements, induced by IR laser light[50] (see Figure 8). The observed intramoleular ligand permutations uniquely correspond to the interconversion of nearest neighbors among the six equivalent C_{2v} structures that are (partly) represented in Figure 3b. The so-called Berry exchange, which would interconvert antipodal C_{2v} structures (situated at opposite ends of the same Q_{t_2} axis), is apparently not taking place under the same activation conditions. The only observed pathways thus precisely correspond to the thermally allowed reaction, which was predicted in Scheme VI.

As shown in some detail in Figures 9 and 10, the Berry exchange is forbidden, since it interconverts two structures characterized by a different ground-state symmetry with respect to the group that is conserved during the process (C_{2v}). In fact the Berry interchange of the two $C_{2v}{}^z$ structures reverses the sign of Q_ζ in eq 15a and hence alters the eigenvector: the $B_1 \leftrightarrow B_2$ process is forbidden. Photochemically however the reaction is predicted—and observed—to be allowed. A topological analysis of this mode selectivity in $Fe(CO)_4$ (as compared to SF_4) is presented elsewhere.[51]

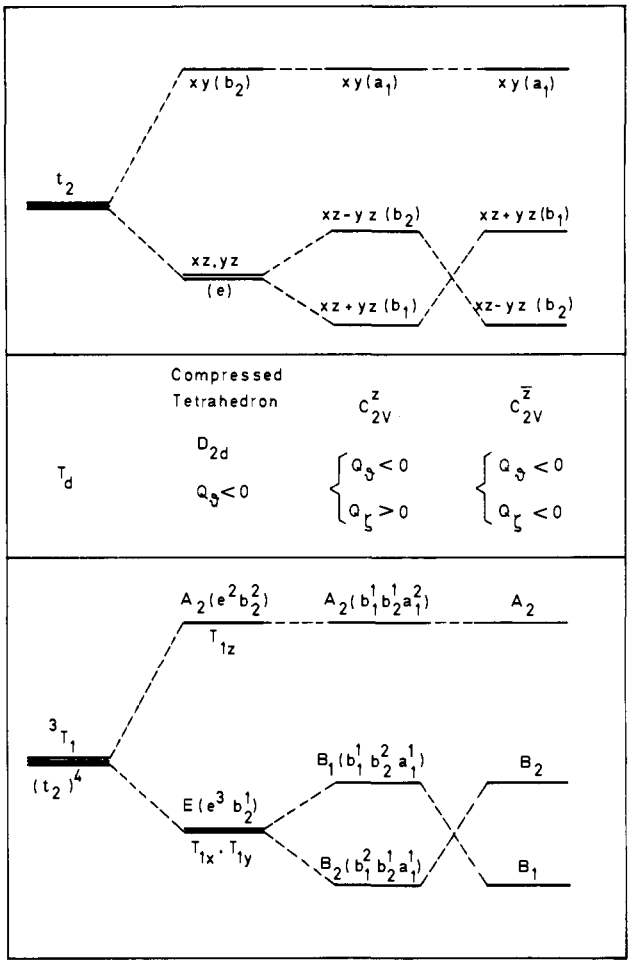

Figure 9. Detailed orbital and state correlation diagrams for JT distorted $Fe(CO)_4$. The relevant distortion coordinates, Q_θ and Q_ζ, are defined in Figure 2. Character conventions for $C_{2v}{}^z$ are specified in ref 25. In the left upper corner are shown the three degenerate starting orbitals of t_2 symmetry. If the tetrahedron is compressed ($Q_\theta < 0$) the t_2 level splits into two components of b_2 and e symmetry. Upon compression the ligands approach the xy coordinate plane. As a result the xy orbital is destabilized while the e orbitals, which have no density in this plane, are lowered in energy. A further symmetry reduction along Q_ζ causes a splitting of the e level into b_1 and b_2 components. The b_1 component ($xz + yz$) has its major density in the σ^{xy} plane (cf. Figure 1), whereas b_2 reaches its maximal density in $\sigma^{x\bar{y}}$. The sign of the splitting can simply be explained, as shown in Figure 10. Obviously if the sign of Q_ζ is reversed, the b level ordering is equally reversed. The lower part of the figure shows a triplet-state correlation diagram, which can immediately be obtained from the orbital correlation by populating the t_2 orbitals by four electrons. The tetrahedral ground state is an open shell $^3T_1$ state. State functions $|T_{1x}\rangle$, $|T_{1y}\rangle$, and $|T_{1z}\rangle$ are specified in eq 27. These functions directly describe the D_{2d} components $|A_2\rangle$ and $|E\rangle$ (see also Figure 5). The C_{2v} components are listed in eq 14. Clearly the interconversion of antipodal C_{2v} structures changes the symmetry of the ground-state eigenvector and is therefore electronically forbidden.

C. Harmonic Force Constants. Unlike all other vibronic contributions in eq 10, the operators corresponding to the harmonic force constants K_e and K_t are totally symmetric; therefore they contain contributions from the completely filled e shell in $e^4t_2{}^n$.

(45) Bacci, H. *J. Phys. Chem. Solids* **1980**, *41*, 1267.
(46) Reinen, D. *Comments Inorg. Chem.* **1983**, *2*, 227.
(47) Burdett, J. K. *Inorg. Chem.* **1981**, *20*, 2607.
(48) Bouman, T. D.; Duncan, C. D.; Trindle, C. *Int. J. Quantum Chem.* **1977**, XI, 399.
(49) McNeish, A.; Poliakoff, M.; Smith, K. P.; Turner, J. J. *J. Chem. Soc., Chem. Commun.* **1976**, 860.
(50) The laser frequency matches the C–O stretching vibrations. Rapid energy transfer to C–M–C bending modes at lower energy is assumed.
(51) Poliakoff, M.; Ceulemans, A. *J. Am. Chem. Soc.* **1984**, *106*, 50.

Table IV

$$\begin{pmatrix} Q_\theta \\ Q_\epsilon \\ Q_\xi \\ Q_\eta \\ Q_\zeta \end{pmatrix} = \begin{pmatrix} K_e + rL_e & (\sqrt{3}s)L_e & a_y a_z W & a_x a_z W & -2a_x a_y W \\ (\sqrt{3}s)L_e & K_e - rL_e & -\sqrt{3}a_y a_z W & \sqrt{3}a_x a_z W & 0 \\ a_y a_z W & -\sqrt{3}a_y a_z W & K_t + pL_t & -2a_x a_y X_t & -2a_x a_z X_t \\ a_x a_z W & \sqrt{3}a_x a_z W & -2a_x a_y X_t & K_t + qL_t & -2a_y a_z X_t \\ -2a_x a_y W & 0 & -2a_x a_z X_t & -2a_y a_z X_t & K_t + rL_t \end{pmatrix}^{-1} \begin{pmatrix} rV_e \\ (-\sqrt{3}s)V_e \\ 2a_y a_z V_t \\ 2a_x a_z V_t \\ 2a_x a_y V_t \end{pmatrix}$$

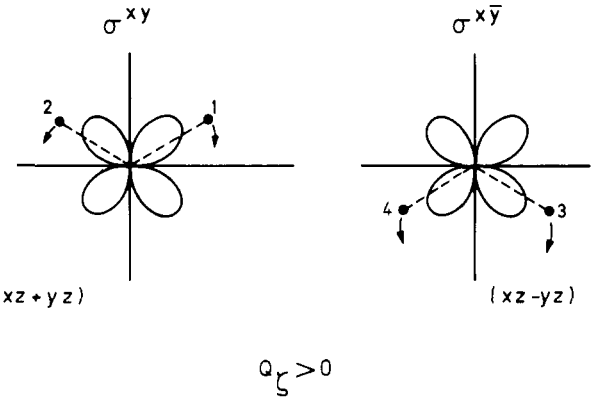

Figure 10. Explanation in a pictorial way of the sign of the C_{2v} splitting in Figure 9. Cross sections shown are along σ^{xy} and $\sigma^{x\bar{y}}$ (cf. Figure 1), containing, respectively, ligands 1 and 2 and ligands 3 and 4. The dots represent ligand positions in a compressed tetrahedron, with angles $\angle 1,2 = \angle 3,4 > 109.47°$. Arrows indicate angular motions that correspond to positive values of the Q_ζ distortion, as defined in Figure 2. The orbital $(1/\sqrt{2})(xz + yz)$ has its major density in the σ^{xy} plane. Obviously, if Q_ζ is activated this orbital will decrease in energy, since the relevant ligands 1 and and 2 are displaced toward a nodal plane. On the contrary, the orthogonal function $(1/\sqrt{2})(xz - yz)$, with major density in $\sigma^{x\bar{y}}$, will be destabilized, as ligands 3 and 4 are moving into directions, where this orbital function reaches its maximal value. In conclusion, for positive values of Q_ζ one expects $(xz + yz)$ to be lower in energy than $(xz - yz)$. For negative values of Q_ζ this orbital order must be reversed.

However, their calculation is substantially simplified, if one realizes that the barycenter energy of the d manifold is not affected by angular displacements. The contribution of an $e^4t_2^n$ configuration is thus exactly outweighed by the contribution of the t_2^{6-n} holes. Using this hole formalism, one obtains for a $e^4t_2^n$ system

$$K_e = K_t = \frac{4}{9R^2}(6 - n)(3\sigma - 4\pi) = \frac{40}{9R^2}(6 - n)Dq \quad (30)$$

where Dq is the classical cubic crystal field parameter. Ligand field calculations thus indicate that harmonic force constants for e and t_2 modes have identical d shell contributions. This quasi-degeneracy is perfectly in line with all evidence from IR spectroscopy on tetrahedral compounds.[52] Nonetheless, it should be kept in mind that the LF approach certainly underestimates the actual values of K_e and K_t, since for instance in a d^{10} system force constants would be predicted to vanish entirely! But one can safely assumes that K_e and K_t are very nearly equal and larger in amplitude than any other nontotally symmetric contribution. This constraint—explicitly considered in section VA—localizes the hypersurface of interest around a central JT origin.

VIII. Conclusion

Somewhat paradoxically, symmetry is seen to play an important role in the understanding of the adiabatic JT effect, the very nature of which is symmetry destruction. The reason is on the one hand that the high symmetry of the unstable JT origin is reflected in the geometry of the surrounding configuration space. On the other hand, the epikernel principle operates in such a way that the JT symmetry destruction is minimized.

While presented as a case study, the present treatment should prove sufficiently general to be carried over to other systems as well. As an example, threefold degenerate octahedral states present a completely analogous problem. The recently observed[53] D_{2h} symmetry of $V(CO)_6$ is equivalent to the C_{2v} symmetry of $Fe(CO)_4$. Therefore, in all probability, the D_{2h} symmetry lowering must be situated in the combined space of the octahedral t_{2g} and e_g modes.

Finally, it should be stressed that we have not paid attention to the role of spin-orbit coupling. While this does not change the symmetry of the configuration space, rather important effects may be expected for the relevant electronic states. Examples are $Ru(CO)_4$ or $Os(CO)_4$ which are presently being investigated.

Table V

$$dQ = (dQ_\theta\ dQ_\epsilon\ dQ_\xi\ dQ_\eta\ dQ_\zeta\ dQ_x\ dQ_y\ dQ_z)$$

$$dq = R(d\theta_1\ d\theta_2\ d\theta_3\ d\theta_4\ \sin\theta_1 d\varphi_1\ \sin\theta_2 d\varphi_2\ \sin\theta_3 d\varphi_3\ \sin\theta_4 d\varphi_4)$$

$$U = \begin{pmatrix} -1/2 & 0 & -1/4 & -1/4 & 1/2 & -\sqrt{3}/4 & \sqrt{3}/4 & 0 \\ -1/2 & 0 & 1/4 & 1/4 & 1/2 & \sqrt{3}/4 & -\sqrt{3}/4 & 0 \\ 1/2 & 0 & 1/4 & -1/4 & 1/2 & \sqrt{3}/4 & \sqrt{3}/4 & 0 \\ 1/2 & 0 & -1/4 & 1/4 & 1/2 & -\sqrt{3}/4 & -\sqrt{3}/4 & 0 \\ 0 & -1/2 & \sqrt{3}/4 & -\sqrt{3}/4 & 0 & -1/4 & -1/4 & 1/2 \\ 0 & -1/2 & -\sqrt{3}/4 & \sqrt{3}/4 & 0 & 1/4 & 1/4 & 1/2 \\ 0 & 1/2 & -\sqrt{3}/4 & -\sqrt{3}/4 & 0 & 1/4 & -1/4 & 1/2 \\ 0 & 1/2 & \sqrt{3}/4 & \sqrt{3}/4 & 0 & -1/4 & 1/4 & 1/2 \end{pmatrix}$$

Acknowledgment. The impetus to the present work has come from a lecture on $Fe(CO)_4$, held by Dr. M. Poliakoff at the 5th International Symposium on the Photochemistry and Photophysics of Coordination Compounds (Paris, Aug 2–5, 1982). A Stanley Kipping Fund has allowed one of us (A.C.) to visit the inorganic chemistry laboratory in Nottingham, U.K. Many stimulating discussions with Prof. J. J. Turner and Dr. M. Poliakoff are gratefully acknowledged. Our research was financially supported by the Belgian Government (Programmatie van het Wetenschapsbeleid). A.C. is indebted to the Belgian National Science Foundation (NFWO) for a research grant.

Appendix

A. The $C_{\Gamma\gamma}$ matrices used in eq 10 contain the Clebsch-Gordan coupling coefficients for the nontotally symmetric squares of T_1 and T_2 states (cf. ref 17). Labeling order of rows and columns corresponds to T_{1x}, T_{1y}, T_{1z} for a T_1 state and $T_{2\xi}$, $T_{2\eta}$, $T_{2\zeta}$ for a T_2 state.[16]

$$C_\theta = \begin{pmatrix} 1/2 & 0 & 0 \\ 0 & 1/2 & 0 \\ 0 & 0 & -1 \end{pmatrix} \qquad C_\epsilon = \begin{pmatrix} -\sqrt{3}/2 & 0 & 0 \\ 0 & \sqrt{3}/2 & 0 \\ 0 & 0 & 0 \end{pmatrix}$$

$$C_\xi = \begin{pmatrix} 0 & 0 & 0 \\ 0 & 0 & -1 \\ 0 & -1 & 0 \end{pmatrix} \qquad C_\eta = \begin{pmatrix} 0 & 0 & -1 \\ 0 & 0 & 0 \\ -1 & 0 & 0 \end{pmatrix} \qquad C_\zeta = \begin{pmatrix} 0 & -1 & 0 \\ -1 & 0 & 0 \\ 0 & 0 & 0 \end{pmatrix}$$

It is interesting to observe that—from a permutational point of view—the matrices of C_ξ, C_η, and C_ζ are more symmetrical than C_θ or C_ϵ. This is because the t_2 coordinates have been constructed in monomial form (for more details, see ref 19).

B. The matrix equation for the configurational coordinates, Q_α, of extremal points as a function of the $\mathbf{a}_i$ eigenvector is shown in Table IV. This equation can directly be derived from the stationary condition in eq 11b. It is defined only if the 5×5 matrix is nonsingular. a_x, a_y, and a_z are the eigenvector components of the vibronic Hamiltonian (eq 11a). To alleviate the notation, the subscript i has been dropped throughout. In addition we define $p = {}^3/_2a_x^2 - {}^1/_2$, $q = {}^3/_2a_y^2 - {}^1/_2$, $r = {}^3/_2a_z^2 - {}^1/_2$, and $s = (a_y^2 - a_x^2)/2$.

(52) Nakamoto, K. "Infrared Spectra of Inorganic and Coordination Compounds"; 2nd ed.; Wiley: New York, 1970.

(53) Bratt, S. W.; Kassyk, A.; Perutz, R. N.; Symons, M. C. R. *J. Am. Chem. Soc.* **1982**, *104*, 490.

C. The angular motion of four ligands in a tetrahedral configuration, at a fixed distance R from the central metal and numbered as in Figure 1, can be decomposed into eight normal coordinates. The five JT-active bending coordinates follow e and t_2 representations and are denoted, respectively, Q_θ, Q_ϵ and Q_ξ, Q_η, Q_ζ. Furthermore there are three bodily rotations, denoted Q_x, Q_y, Q_z, which transform as a t_1 representation. Let $d\theta_i$ and $\sin\theta_i d\varphi_i$ represent infinitesimal angular displacement of ligand L_i in a Cartesian frame as in Figure 1. Equation 24 in the text can now be specified as in Table V. As an example Figure 2 represents the ligand motion associated with positive values of Q_θ and Q_ζ.

Effects of Chemical Substitution on Polymer Band Gaps: Transferability of Band-Edge Energies

John P. Lowe* and Sherif A. Kafafi

Contribution from the Department of Chemistry, Davey Laboratory, The Pennsylvania State University, University Park, Pennsylvania 16802. *Received December 5, 1983*

Abstract: Perturbation theory is used to clarify the effects of chemical substitution on π-band-edge energies in conjugated polymers. One can roughly estimate (without computation) the effect of chemical substitution on computed (extended Hückel) π band-edge energies, hence upon π band gaps. Furthermore, once an edge energy is actually computed for one polymer, it is, in many cases, quantitatively transferable to substitutionally related polymers. This allows π-band-gap energies to be predicted quite accurately for systems not yet studied theoretically. The transferability phenomenon does not appear to be nullified by bond-length alternation or to be dependent upon choice of theoretical method.

I. Introduction

During the past decade, conjugated polymers have become the subject of great research activity.[1-3] This interest is due to the discovery that the electrical conductivity of a large number of organic polymers, such as poly(acetylene),[4,5] poly(*p*-phenylene),[6] and poly (*p*-phenylene sulfide),[7] can be increased by 12–18 orders of magnitude up to the metallic level. This increase in conductivity is achieved by doping.

The increased experimental activity in conjugated polymers[8-10] has led to intensified efforts to achieve theoretical understanding using quantum chemical calculations. Whangbo and Hoffmann[11] have examined a variety of conjugated one- and two-dimensional polymers using the extended Hückel (EH) method. They have explored how band-gap sizes and the occurrence of partially filled bands are related to unit cell constitution and the geometrical disposition of the atoms in the unit cell. Duke et al.,[12-15] using the spectroscopically parameterized CNDO-S3 model, have studied the relationships between macromolecular architecture and characteristic features in the photoemission spectra of polymers. Recently, Brēdas et al.,[16-19] using a valence effective Hamiltonian (VEH) technique, have examined a number of organic polymers in order to define the variations in molecular, crystallographic, and defect structures that are compatible with high conductivity.

In this paper, we consider the effects of chemical substitution on π-band-edge energies in conjugated polymers. We find that it is possible to predict these effects semiquantitatively and hence to estimate, without calculation, the size of the π-band gaps in substitutionally related polymers. Furthermore, we show that calculated π-band-edge energies are transferable among related systems.

Throughout this paper, we will use the extended Hückel crystal orbital (EHCO)[11,20] method to illustrate our conclusions concerning the trans polymers shown in Figure 1.

The paper is structured as follows. In section II, we consider the effects of chemical substitution on the π-band-edge energies of regular *trans*-poly(acetylene). The effect of subsequent bond-length alternation is examined in section III. An illustration is given, in section IV, of the transferability of band-edge energies from known polymers to a new one, and the applicability of these ideas to SCF calculations is considered in section V.

II. Effect of Substitution on π-Band-Edge Energies

Backbone Substitution: Regular Poly(acetylene), Poly(methine imine), and Poly(sulfur nitride). First, we consider poly(acetylene)

(1) Kertesz, M. *Adv. Quantum Chem.* **1982**, *15*, 161.
(2) "Molecular Metals"; Hatfield, W. E., Ed.; Plenum Press: New York, 1979; Vol. 1.
(3) Andrē, J. M. *Adv. Quantum Chem.* **1980**, *12*, 65.
(4) Etemad, S.; Heeger, A. J.; McDiarmid, A. G. *Annu. Rev. Phys. Chem.*, **1982**, *33*, 443.
(5) Salaneck, W. R.; Thomas, H. C.; Duke, C. B.; Paton, A.; Plummer, E. W.; Heeger, A. J.; MacDiarmid, A. G. *J. Chem. Phys.* **1979**, *71*, 2044.
(6) Ivory, D. M.; Miller, G. G.; Sowa, J. M.; Shacklette, L. W.; Chance, R. R.; Baughman, R. H. *J. Chem. Phys.* **1979**, *71*, 1506.
(7) Chance, R. R.; Shacklette, L. W.; Miller, G. G.; Ivory, D. M.; Sowa, J. M.; Elsenbaumer, R. L.; Baughman, R. H. *J. Chem. Soc., Chem. Commun.* **1980**; 348.
(8) Fabish, T. J. *CRC Crit. Rev. Solid State Mater. Sci.*, **1979**, 383.
(9) Baughman, R. H.; Brēdas, J. L.; Chance, R. R.; Eckhardt, H.; Elsenbaumer, R. L.; Ivory, D. M.; Miller, G. G.; Preiziosi, A. F.; Shacklette, L. W. "Conductive Polymers"; Seymour, R. B., Ed., Plenum Press: New York, 1981; p 137.
(10) Duke, C. B. "Extended Linear Chain Compounds"; Miller, J. S., Ed.; Plenum Press: New York, 1982; Vol. 2, p 59.
(11) Whangbo, M. H.; Hoffmann, R.; Woodward, R. B. *Proc. R. Soc. London, Ser. A*, **1979**, *366*, 23.
(12) Duke, C. B.; Paton, A.; Salaneck, W. R. *Mol. Cryst. Liq. Cryst.* **1982**, *83*, 177.
(13) Ford, W. K.; Duke, C. B.; Paton, A. *J. Chem. Phys.* **1982**, *77*, 4564.
(14) Ford, W. K.; Duke, C. B.; Paton, A. *J. Chem. Phys.* **1983**, *78*, 4734.
(15) Duke, C. B.; Paton, A. "Conductive Polymers"; Seymour, R. B., Ed., Plenum Press: New York, 1981.
(16) Brēdas, J. L.; Chance, R. R.; Baughman, R. H.; Silbey, R. *Int. J. Quantum Chem. Symp.* **1981**, *15*, 231.
(17) Brēdas, J. L.; Chance R. R.; Baughman, R. H.; Silbey, R. *J. Chem. Phys.* **1982**, *76*, 3673.
(18) Brēdas, J. L.; Thēmans, B.; Andrē, J. M. *J. Chem. Phys.* **1983**, *78*, 6137.
(19) Baughman, R. H.; Bredās, J. L.; Chance, R. R.; Elsenbaumer, R. L.; Shacklette, L. W. *Chem. Rev.* **1982**, *82*, 209.
(20) Whangbo, M. H.; Hoffmann, R. *J. Am. Chem. Soc.* **1978**, *100*, 6093.

0002-7863/84/1506-5837$01.50/0